iScience

CellPress

Article

EGFR Controls Hair Shaft Differentiation in a p53-Independent Manner

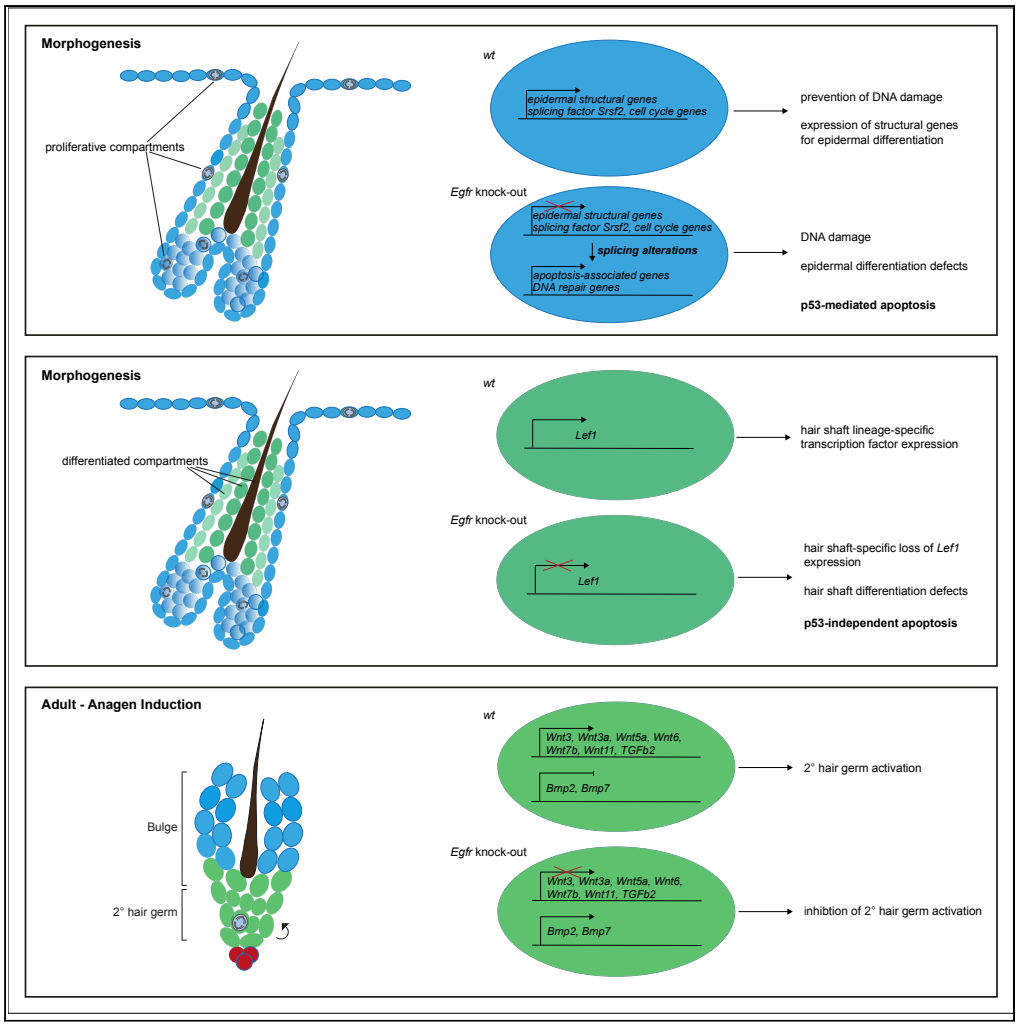

Nicole Amberg, Panagiota A. Sotiropoulou, Gerwin Heller, ..., Temenuschka Baykuscheva-Gentscheva, Cedric Blanpain, Maria Sibilia

maria.sibilia@meduniwien.ac.at

HIGHLIGHTS

EGFR has compartment-specific functions in distinct keratinocyte populations

EGFR exerts p53-dependent control on DNA integrity in proliferative keratinocytes

EGFR controls epithelial hair lineage differentiation in a p53-independent manner

EGFR contributes to onset of anagen induction in adult hair follicle stem cells

Amberg et al., iScience *15*, 243–256
May 31, 2019
https://doi.org/10.1016/j.isci.2019.04.018

iScience

CellPress

Article

EGFR Controls Hair Shaft Differentiation in a p53-Independent Manner

Nicole Amberg,[1,5] Panagiota A. Sotiropoulou,[2,6] Gerwin Heller,[3] Beate M. Lichtenberger,[1,7] Martin Holcmann,[1] Bahar Camurdanoglu,[1] Temenuschka Baykuscheva-Gentscheva,[1] Cedric Blanpain,[2,4] and Maria Sibilia[1,8,*]

SUMMARY

Epidermal growth factor receptor (EGFR) signaling controls skin development and homeostasis in mice and humans, and its deficiency causes severe skin inflammation, which might affect epidermal stem cell behavior. Here, we describe the inflammation-independent effects of EGFR deficiency during skin morphogenesis and in adult hair follicle stem cells. Expression and alternative splicing analysis of RNA sequencing data from interfollicular epidermis and outer root sheath indicate that EGFR controls genes involved in epidermal differentiation and also in centrosome function, DNA damage, cell cycle, and apoptosis. Genetic experiments employing *p53* deletion in EGFR-deficient epidermis reveal that EGFR signaling exhibits *p53*-dependent functions in proliferative epidermal compartments, as well as *p53*-independent functions in differentiated hair shaft keratinocytes. Loss of EGFR leads to absence of LEF1 protein specifically in the innermost epithelial hair layers, resulting in disorganization of medulla cells. Thus, our results uncover important spatial and temporal features of cell-autonomous EGFR functions in the epidermis.

INTRODUCTION

Skin morphogenesis is a complex process requiring the spatial and temporal orchestration of distinct molecular signaling pathways to ensure correct development of epidermal lineages such as interfollicular epidermis (IFE), hair follicles (HF), and sebaceous glands. Initiation of HF development is mainly conducted by β-catenin and SHH signaling (Huelsken et al., 2001; Blanpain and Fuchs, 2009; Hsu et al., 2014), resulting in formation of hair placodes between embryonic day (E)15 and E17 (Tumbar, 2012). After the critical step of placode formation, SHH stimulates proliferation of cells within this structure, which then grow down into the dermis as hair germs and further develop into hair pegs between E17 and E18 (Hsu et al., 2014). Continuous growth of the hair peg leads to the formation of a mature HF, which is constituted of highly proliferative progenitor cells, the so-called matrix, at the bottom. Progeny of the matrix gives rise to the distinct differentiated epithelial cell layers, which comprise the hair or function in hair guidance (Hsu et al., 2014; Adam et al., 2018). The cell layers from the outer to innermost layer are outer root sheath (ORS), companion layer, three layers of inner root sheath (IRS), cuticle, cortex, and medulla. WNT/β-catenin and bone morphogenetic protein (BMP) signaling were shown to orchestrate hair layer differentiation by temporal layering of signaling effectors (Adam et al., 2018). Impairment in the formation of solely one layer is sufficient to induce the collapse of the hair shaft and sustained disruption of hair development (DasGupta and Fuchs, 1999; Kaufman, 2003).

Besides instructive Wnt/β-catenin and BMP signaling pathways, epidermal growth factor receptor (EGFR) signaling strongly contributes to skin development and homeostasis of mice and humans. Mice completely lacking EGFR are born with open eyes and display severe skin defects, including a pronounced delay in HF development (Miettinen et al., 1995; Sibilia and Wagner, 1995; Threadgill et al., 1995). Expression of a dominant-negative mutant of EGFR in keratinocytes (Murillas et al., 1995) and hair transplantation experiments (Hansen et al., 1997) revealed that EGFR-deficient HFs are able to progress through morphogenesis for about 2 weeks after birth, but then fail to enter catagen. Similarly, humanized EGFR mice ($hEGFR^{KI/KI}$) exhibit impaired HF morphogenesis, alterations in morphology and distribution of HFs, and a failure in anagen to catagen transition owing to inefficient expression of the *hEGFR* in the skin (Sibilia et al., 2003). At postnatal day (P)90, $hEGFR^{KI/KI}$ mice mostly contained degenerated HFs with thin hair cell layers, which were partly destroyed. Later, studies in conditional knockout mice lacking the EGFR specifically in the epidermal lineage (Nagao et al., 2012; Lichtenberger et al., 2013; Mascia et al., 2013; Bichsel et al., 2016) confirmed that loss of EGFR in keratinocytes is sufficient to induce skin differentiation defects, catagen block, loss of the HF niche, and baldness. Moreover, epidermis-specific EGFR knockout results in severe

[1]Institute of Cancer Research, Department of Internal Medicine I, Comprehensive Cancer Center, Medical University of Vienna, Vienna 1090, Austria

[2]Interdisciplinary Research Institute (IRIBHM), Université Libre Bruxelles, Bruxelles 1070, Belgium

[3]Department of Medicine I, Comprehensive Cancer Center, Clinical Division of Oncology, Medical University of Vienna, Vienna 1090, Austria

[4]WELBIO, Interdisciplinary Research Institute (IRIBHM), Université Libre Bruxelles, Bruxelles 1070, Belgium

[5]Present address: IST Austria, Klosterneuburg 3400, Austria

[6]Present address: Celyad, Mont St. Guibert 1435, Belgium

[7]Present address: Department of Dermatology, Skin & Endothelium Research Division (SERD), Medical University of Vienna, Vienna 1090, Austria

[8]Lead Contact

*Correspondence: maria.sibilia@meduniwien.ac.at

https://doi.org/10.1016/j.isci.2019.04.018

skin inflammation and confers high susceptibility to *S. aureus* infections. Similar phenotypes have also been observed in cancer patients receiving anti-EGFR therapies (Lichtenberger et al., 2013; Mascia et al., 2013). In contrast, mice harboring either the naturally occurring EGFR mutation *waved2* (Luetteke et al., 1994) or the transforming growth factor (TGF)-α mutation *waved1* (Crew, 1933; Luetteke et al., 1993) only show a mild phenotype characterized by wavy hair coat and whiskers but otherwise normal physiology. TGFα shows specific expression in cells of the IRS (Luetteke et al., 1993), suggesting an important role of EGFR signaling in the control of epithelial hair layer development and hair shape, whereas EREG and AREG have been shown to affect sebocyte numbers or sebaceous gland size (Dahlhoff et al., 2014; Li et al., 2016).

So far it has been poorly investigated how much the skin inflammation developing in the absence of epidermal EGFR affects the stem cell compartments thus aggravating the resulting phenotypes. Therefore in this study we employed conditional mouse models allowing us to dissect the cell-autonomous functions of EGFR signaling in distinct keratinocyte and stem cell compartments independently of the non-cell-autonomous contribution of inflammation. Our results indicate that EGFR signaling ensures DNA integrity in proliferative compartments, where accumulation of DNA damage results in TP53-dependent cell death. Moreover, we demonstrate that EGFR controls transcription factor expression in the innermost epithelial hair lineages, which is required for hair shaft differentiation.

RESULTS

Previous studies have shown that skin-specific genetic ablation of EGFR during murine embryonic development causes profound defects of HF morphogenesis, but so far lacked detailed mechanistic analysis. Developing HFs need to go through several sequential phases to give rise to a mature HF (Figure 1A). To specifically investigate the function of EGFR signaling during the specification and growth phase of HF morphogenesis, $Egfr^{fl/fl}$ mice (Natarajan et al., 2007) were crossed with *K5Cre* transgenic mice to generate mice lacking the EGFR already during embryonic development in the epidermal lineage ($Egfr^{\Delta ep}$ mice, Figures S1A and S1B; Table S3; Lichtenberger et al., 2013). Time course analysis during the growth, catagen, and telogen phases of HFs showed that $Egfr^{\Delta ep}$ mice present a significant delay in HF growth (Figures 1B–1D), a catagen block (Figures 1C and 1D), and hair shape alterations (Figure S1C).

EGFR Deficiency Does Not Result in Alterations of HF Specification during Morphogenesis

First, we analyzed HF specification at late embryonic time points to investigate whether lack of EGFR may impair early HF development. Staining for E-Cadherin confirmed correct anterior-to-posterior orientation of hair pegs as detected by the absence of E-Cadherin expression at the anterior part of the HF (Muller-Rover et al., 1999; Devenport and Fuchs, 2008) in both control and $Egfr^{\Delta ep}$ mice (Figure 1E). Furthermore, the angle between IFE and HF was mainly similar between control and $Egfr^{\Delta ep}$ mice (Figures 1F and 1G). Despite HF growth differences, we did not find differences in expression of hair follicle stem cell (HFSC) fate factors in newborn mice: histological stainings for the HF progenitor/stem cell markers P-Cadherin and LHX2 (Folgueras et al., 2013) (Figure 1H) and the NFATc1-positive or Nephronectin (NPTN)-positive prospective bulge region in HF (Horsley et al., 2008; Fujiwara et al., 2011) (Figures 1I and 1J) showed robust expression and correct location of those factors in embryonic and newborn skin of $Egfr^{\Delta ep}$ mice. These results demonstrate that EGFR is not required to induce embryonic HFSC specification but exerts its function on proper HF morphogenesis during the growth phase.

EGFR Controls Genes Required for Epidermal Differentiation and DNA Integrity

To uncover the genes involved in EGFR-mediated regulation of the growth of epidermal lineages, RNA sequencing (RNA-seq) analysis was performed on sorted IFE and ORS cells from postnatal day (P)2 mice. To label ORS cells we crossed $Egfr^{\Delta ep}$ with $LGR5Cre^{ERT2}GFP$ mice to make use of LGR5-driven GFP expression as an ORS marker (Jaks et al., 2008), whereas IFE cells were defined as SCA-I^{hi} $ITGA6^{hi}$ cells (Figures S2A–S2C). The time point P2 was chosen, because at that stage there was still no immune cell infiltration in the skin of $Egfr^{\Delta ep}$ pups (Figure S2D), but a delay in HF growth was already detectable (Figure 1B). We observed reduced GFP expression in ORS cells of $Egfr^{\Delta ep}$ mice at P2, although the total fraction of LGR5-expressing cells was similar to control mice (Figures S2E–S2H). RNA-seq analysis showed strong expression of *Egfr*, *Erbb2,* and *Erbb3* in IFE and ORS of control mice, whereas there was no expression of *Erbb4*. Furthermore, we observed no or only low EGFR ligand expression in the different epidermal compartments, like low *Epgn* expression in the IFE, and low *Hb-egf* in both IFE and ORS (Figure S2I).

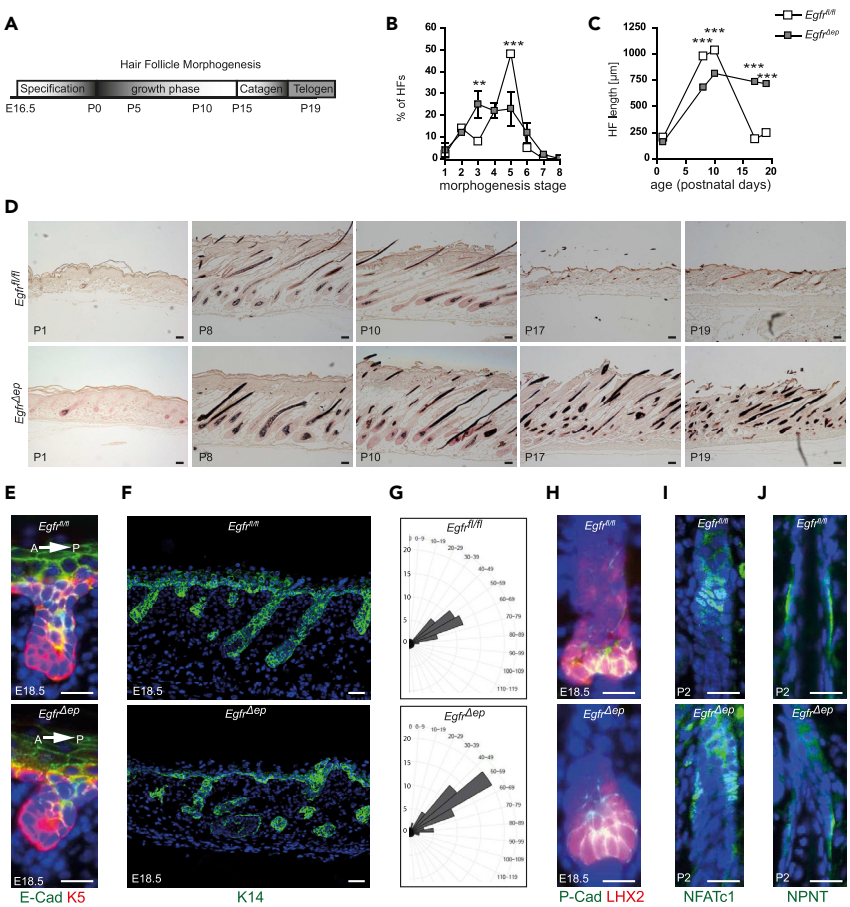

Figure 1. EGFR Deficiency Does Not Result in Alterations of HF Specification during Morphogenesis

(A) Schematic time course of HF morphogenesis.

(B) HF morphogenesis staging from control and *Egfr*$^{\Delta ep}$ mice at P1. Bars show analysis of 15–20 follicles per mouse from n = 3 mice per genotype. Data are represented as mean ± SD. p values less than 0.05 were considered significant, with **p < 0.01, ***p < 0.001 as determined by multiple t test using two-stage linear step-up procedure of Benjamini, Krieger, and Yekutieli with Q = 1%.

(C) Quantification of HF length from control and *Egfr*$^{\Delta ep}$ mice at indicated time points. Bars show analysis of 15–20 follicles per mouse from n = 3 mice per genotype. Data are represented as mean ± SD. p values less than 0.05 were considered significant, with ***p < 0.001 as determined by multiple t test using two-stage linear step-up procedure of Benjamini, Krieger, and Yekutieli with Q = 1%.

(D) Fontana-Masson stainings of back skin sections from control and *Egfr*$^{\Delta ep}$ mice at indicated time points. Scale bars, 50 µm.

(E) Immunofluorescence staining for E-Cadherin (green), K5 (red), and nuclei (blue) from control, and *Egfr*$^{\Delta ep}$ mice at E18.5. Arrow indicates anterior-to-posterior orientation of skin section. A, anterior; P, posterior.

(F) Immunofluorescence staining for K14 (green) and nuclei (blue) from E18.5 control and *Egfr*$^{\Delta ep}$ mice.

(G) Polar plots of angles between IFE and anterior side of HFs from E18.5 control and *Egfr*$^{\Delta ep}$ mice. Plots show analysis of 8–12 follicles per mouse from n = 3 mice per genotype. Data represent the absolute number of HFs measured at indicated angle ranges.

(H) Immunofluorescence staining for P-Cadherin (green), LHX2 (red), and nuclei (blue) from control and *Egfr*$^{\Delta ep}$ mice at E18.5.

(I) Immunofluorescence staining for NFATc1 (green) and nuclei (blue) from control and *Egfr*$^{\Delta ep}$ mice at P2.

(J) Immunofluorescence staining for Nephronectin (NPNT, green) and nuclei (blue) from control and *Egfr*$^{\Delta ep}$ mice at P2. Scale bars, 20 µm unless otherwise stated. See also Figure S1.

Analysis of differentially expressed genes between control and *Egfr*$^{\Delta ep}$ mice revealed that loss of EGFR significantly affects the expression of structural genes (*Spink5*, *Lce1e1*, *Flg*, *Sprr1a*, *Klk7*, *Gjb4*), as well as of genes regulating cell cycle and apoptosis (*Perp*, *Cep120*, *Klhdc5*, *Egr1*, *Fos*) in IFE or ORS cells (Figures 2A–2D; Table S1A).

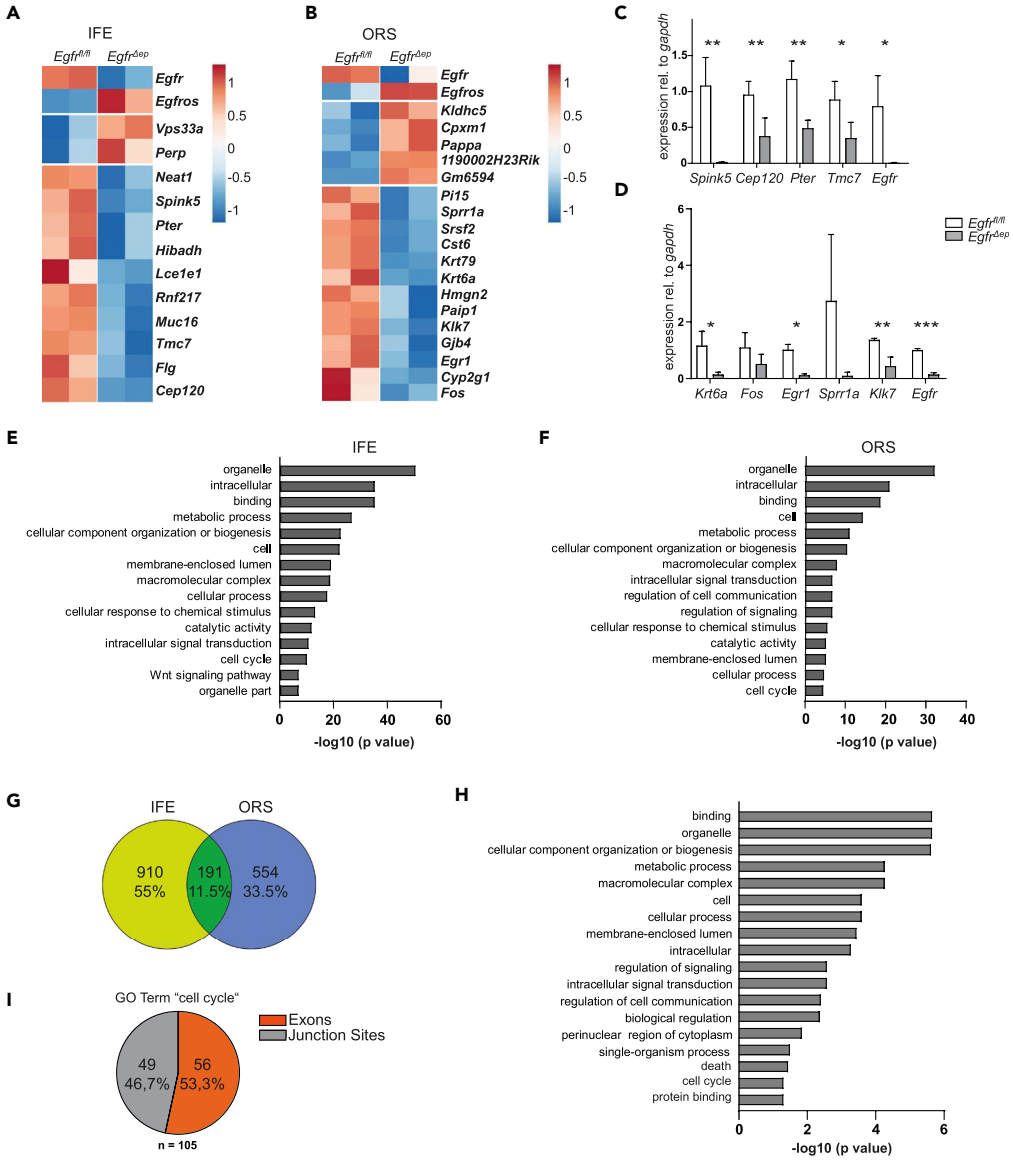

Figure 2. EGFR Controls a Variety of Genes Required for Epidermal Differentiation and DNA Integrity

(A) Heatmap of significantly deregulated genes in P2 fluorescence-activated cell sorted IFE from control and *Egfr*$^{\Delta ep}$ mice. Each column represents one mouse.

(B) Heatmap of significantly deregulated genes in P2 fluorescence-activated cell sorted ORS from control and *Egfr*$^{\Delta ep}$ mice. Each column represents one mouse.

(C) qRT-PCR from randomly chosen target genes identified by RNA-seq from P2 IFE. Bars show data from n = 3–5 mice per genotype. Data are represented as mean ± SD. p values less than 0.05 were considered significant, with *p < 0.05, **p < 0.01 as determined by Student's t test.

(D) qRT-PCR from randomly selected target genes identified by RNA-seq from P2 ORS. Bars show data from n = 3–5 mice per genotype. Data are represented as mean ± SD. p values less than 0.05 were considered significant, with *p < 0.05, **p < 0.01, ***p < 0.001 as determined by Student's t test.

(E) Bar graph of the top 15 GO terms obtained from alternative splicing analysis from IFE keratinocytes.

(F) Bar graph of the top 15 GO terms obtained from alternative splicing analysis from ORS keratinocytes.

(G) Venn diagram of alternative splicing targets from P2 IFE and ORS cells.

(H) Bar graph of the significantly enriched GO terms obtained from overlapping genes displaying alternatively spliced exons or junction sites from IFE and ORS keratinocytes.

(I) Pie chart of the ratio of alternatively used exons and junction sites of genes within the GO term "cell cycle."

See also Figure S2 and Tables S1A–S1F.

EGFR Controls Alternative Splicing, which Regulates Centrosome Function and DNA Integrity

As the list of differentially expressed genes included a variety of targets that were either already shown to be directly linked to EGFR signaling, such as *Flg* (Franzke et al., 2012), or belonged to an expected biological process, namely, epidermal development, we focused on novel targets not yet reported to regulate epidermal integrity in the context of EGFR signaling. One of those target genes was *Srsf2* (Figure 2B). The product of this gene is required for the formation of the earliest ATP-dependent splicing complex and contributes to constitutive as well as alternative splicing (Graveley and Maniatis, 1998). To functionally investigate whether lack of EGFR might affect mRNA splicing, we analyzed our RNA-seq datasets for alternative exon usage employing JunctionSeq (Hartley and Mullikin, 2016). For both compartments, IFE and ORS, we detected a high number of alternative transcripts upon comparison of control and EGFR-deficient keratinocytes. Importantly, these genes group into distinct GO terms like "intracellular signal transduction," "Wnt pathway," "cell cycle," or "organelle part" (Figures 2E and 2F, Table S1B).

To gain more specific information from the large amount of alternatively used exons and junction sites, we focused on the 191 (11.5%) affected overlapping genes between IFE and ORS (Figure 2G, Table S1C). GO term analysis on those overlapping targets elucidated that EGFR is required to control the "perinuclear region of cytoplasm," "cell cycle," and "death" in both IFE and ORS (Figure 2H, Table S1D). Deeper investigation of the genes belonging to the term "cell cycle" revealed a high number of genes important in centrosome function and DNA damage repair, e.g., *Cntrl*, *Cep192*, *Clspn*, and *Bub1b* (Table S1E), and an almost equal number of differentially used exons and junction sites (Figure 2I, Table S1F).

EGFR Regulates Proliferation and Prevents DNA Damage in Epidermal Lineages

As both global gene expression and alternative splicing analysis identified genes involved in cell cycle, centrosome function, and DNA damage response we hypothesized that a strong disbalance of cell turnover or survival and apoptosis could explain the growth delay of EGFR-deficient HFs. In light of previous reports on an important function of EGFR in promotion of proliferation (Hansen et al., 1997; Bol et al., 1998; Xie et al., 1999; Kiguchi et al., 2000; Lichtenberger et al., 2010), we functionally tested whether EGFR is required for regulating the proliferation rate of distinct keratinocyte populations. RNA-seq analysis showed downregulation of early growth response 1 (*Egr1*) in the ORS of $Egfr^{\Delta ep}$ mice (Figure 2B). It was previously demonstrated that *Egr1* is a downstream target of ERK signaling and involved in cell growth and proliferation (Mayer et al., 2009; Tarcic et al., 2011). We confirmed EGR1 protein absence in the ORS (Figure 3A), as well as strongly reduced phospho-ERK1/2 selectively in ORS cells of EGFR-deficient skin (Figure 3B). In addition, bromodeoxyuridine (BrdU) pulse-chase experiments showed reduced BrdU incorporation into EGFR-deficient ORS cells after 24h (Figures 3C and S3A), providing evidence that EGFR signaling in the ORS is required to induce the ERK signaling cascade, leading to *Egr1* induction and cell growth or proliferation. To address whether absence of EGFR also affects proliferation in the IFE, back skin sections from various time points (P5, P8, P10) were stained for Ki67 and additionally analyzed by flow cytometry after a 4h BrdU pulse. Our results show that both numbers of $Ki67^+$ cells and $BrdU^+$ cells are reduced in IFE of $Egfr^{\Delta ep}$ mice when compared with control mice (Figures 3D, 3E, and S3B). These data confirm previous findings (Bol et al., 1998; Xie et al., 1999; Kiguchi et al., 2000; Lichtenberger et al., 2010) and provide more detailed insights into the important role of EGFR in promoting proliferation of the epidermal lineage.

Detailed depiction of exon usage of Centriolin (*Cntrl*) (Figure S3C) shows that EGFR-deficient keratinocytes preferentially skip exons 11, 15, and 16. Exon 11 encodes an alternative 3′ UTR and leads to a shorter transcript, which is known as a 110-kDa variant of *Cntrl* termed *Cep110*. Skipping of the alternative part of exon 11 leads to an increase in full-length transcript, encoding a 270-kDa variant of *Cntrl*, including a domain required for centrosome localization (Szebenyi et al., 2007). Exons 15 and 16 contribute to the stathmin domain of CNTRL, which is involved in regulation of mitotic spindle assembly. Further investigation of Claspin (*Clspn*) mRNA shows that $Egfr^{\Delta ep}$ mice skip exon 12 (Figure S3D). Claspin is required for cell-cycle arrest in response to DNA damage via activation of CHK1 (Lee et al., 2003). Interestingly, exon 12 encodes a protein region involved in forming the CHK1-activating domain (CKAD), suggesting that exon skipping leads to reduced binding of CLSPN to CHK1 and subsequently to reduced clearance of DNA damage.

To test this hypothesis, we investigated centrosome numbers, DNA damage, and apoptosis. Pericentrin stainings of primary keratinocytes revealed an increased fraction of EGFR-deficient keratinocytes displaying more than two centrosomes (Figures 3F and 3G). Moreover, we observed nuclear fragmentation in

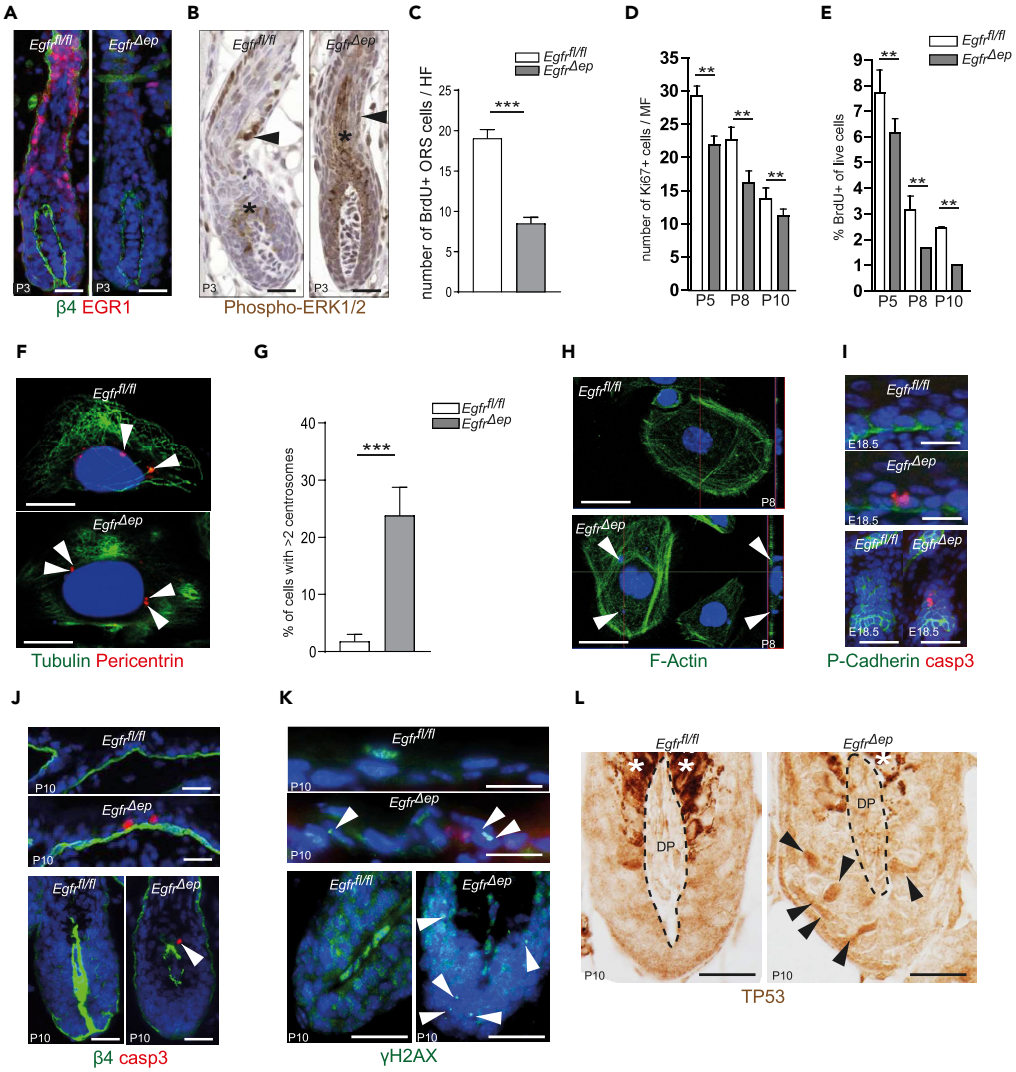

Figure 3. EGFR Controls Cell Proliferation as well as Centrosome Function and DNA Integrity

(A) Immunofluorescence staining for ITGB4 (green), EGR1 (red), and nuclei (blue) from P3 control and *Egfr*$^{\Delta ep}$ mice.

(B) Immunohistochemistry staining for phospho-ERK1/2 from P3 control and *Egfr*$^{\Delta ep}$ mice. Asterisk indicates hair pigmentation.

(C) Quantification of BrdU^{+} ORS cells of P2 mice 24h after BrdU pulsing. Bars show analysis of 10 follicles per mouse from n = 4 mice per genotype. Data are represented as mean ± SD. p values less than 0.05 were considered significant, with ***p < 0.001 as determined by Student's t test.

(D) Quantification of the number of Ki67^{+} IFE nuclei from frozen back skin sections from control and *Egfr*$^{\Delta ep}$ mice at indicated time points. MF, microscopic field. Bars show analysis of 6 microscopic fields per mouse from n = 3 mice per genotype. Data are represented as mean ± SD. p values less than 0.05 were considered significant, with **p < 0.01 as determined by Student's t test.

(E) Quantification of the number of BrdU^{+} cells from epidermal cell suspensions analyzed by fluorescence-activated cell sorting from control and *Egfr*$^{\Delta ep}$ mice at indicated time points. Bars show analysis of n = 3 mice per genotype. Data are represented as mean ± SD. p values less than 0.05 were considered significant, with **p < 0.01 as determined by Student's t test.

(F) Immunofluorescence staining for Tubulin (green), Pericentrin (red), and nuclei (blue) from primary keratinocytes derived from control and *Egfr*$^{\Delta ep}$ mice. Arrows point to centrosomes. Scale bars, 5 μm.

(G) Quantification of the percentage of primary keratinocytes harboring more than two centrosomes. Bars show analysis of 15 cells per mouse from n = 3 mice per genotype. Data are represented as mean ± SD. p values less than 0.05 were considered significant, with ***p < 0.001 as determined by Student's t test.

(H) Immunofluorescence staining for F-Actin (green) and nuclei (blue) of primary keratinocytes derived from P8 control and *Egfr*$^{\Delta ep}$ mice. Arrows highlight nuclear fragments. Scale bars, 5 μm.

Figure 3. *Continued*

(I) Immunofluorescence staining for P-Cadherin (green), activated caspase 3 (red), and nuclei (blue) from control and $Egfr^{\Delta ep}$ mice at E18.5, showing IFE (top) and HF (bottom).

(J) Immunofluorescence staining for ITGB4 (green), activated caspase 3 (red), and nuclei (blue) from control and $Egfr^{\Delta ep}$ mice at P10, showing IFE (top) and HF matrix (bottom). Arrow highlights an apopotic cell.

(K) Immunofluorescence staining for γH2AX (green) and nuclei (blue) from control and $Egfr^{\Delta ep}$ mice at P10, showing IFE (upper panel) and HF matrix (lower panel). Arrows highlight spots of DNA damage.

(L) Immunohistochemical staining of TP53 on sections of P10 control and $Egfr^{\Delta ep}$ mice, showing HF matrix. Asterisk indicates hair pigmentation, delineated area marks dermal papilla (DP).

Scale bars, 20 μm unless otherwise stated. See also Figure S3.

keratinocytes lacking EGFR (Figure 3H). As both, WT and $Egfr^{\Delta ep}$ keratinocyte cultures, were negative for the differentiation marker K1, we exclude that fragmentation of nuclei might be due to accelerated differentiation of EGFR-deficient keratinocytes (Figure S3E). To analyze whether loss of DNA integrity is accompanied by increased cell death, we stained back skin sections for active caspase 3. Apoptotic cells were detected in the IFE and hair pegs of E18.5 epidermis (Figure 3I) as well as in P10 IFE and matrix of $Egfr^{\Delta ep}$ mice (Figure 3J). Furthermore, staining for the DNA damage marker γH2AX uncovered a high number of γH2AX foci in skin of $Egfr^{\Delta ep}$ mice, but not in control mice (Figure 3K). The presence of DNA damage was accompanied by stabilization and accumulation of TP53 in nuclei of matrix cells from $Egfr^{\Delta ep}$ mice (Figure 3L). These data demonstrate that absence of EGFR leads to accumulation of DNA damage, which subsequently induces TP53 stabilization and apoptosis.

Apoptosis in IFE and Matrix Is TP53 Dependent, Whereas Loss of Inner Hair Layers Is TP53 Independent

To investigate whether TP53-induced cell death causes impaired HF development in $Egfr^{\Delta ep}$ mice, we crossed $Egfr^{\Delta ep}$ mice with $p53^{fl/fl}$ mice to generate $Egfr/p53^{\Delta ep}$ mice (Figures S4A and S4B). Surprisingly, $Egfr/p53^{\Delta ep}$ mice presented the same phenotype as $Egfr^{\Delta ep}$ mice: skin and hair alterations, reduced survival, and strong skin inflammation (Figures S4C–S4E). However, deletion of TP53 abolished apoptosis in IFE and matrix cells in $Egfr^{\Delta ep}$ mice at P10 (Figures 4A–4D), suggesting a TP53-dependent mechanism for cell death in these highly proliferative epidermal compartments. Upon closer investigation of other epithelial compartments in the epidermal lineage, we also detected apoptotic cells in the hair shaft of $Egfr^{\Delta ep}$ mice, which were, however, not affected by additional TP53 deletion (Figures 4E and 4F), providing evidence for a TP53-independent apoptotic mechanism in postmitotic cells. We could also confirm the presence of apoptosis in innermost hair layers, such as medulla cells, by transmission electron microscopy (Figure 4G). To characterize whether apoptosis in the hair shaft affects the differentiation of epithelial hair layers in mice lacking epidermal EGFR, we stained for hair-layer-specific keratins in control, $Egfr^{\Delta ep}$ mice, and $Egfr/p53^{\Delta ep}$ mice. Both $Egfr^{\Delta ep}$ mice and $Egfr/p53^{\Delta ep}$ mice exhibited onset of hair layer differentiation, but displayed an early loss of those layers (Figure 4H). These data indicate TP53-dependent cell death in proliferative keratinocytes as well as a TP53-independent mechanism of apoptosis in the non-proliferative, differentiated cells of the hair shaft upon lack of EGFR signaling.

EGFR Controls Hair Lineage Transcription Factor Expression

To investigate whether transcription factors involved in hair layer differentiation showed altered expression upon EGFR deletion, we stained for IRS-specific transcription factor GATA-3, as well as for IRS- and HS-specific factor LEF1 (Merrill, 2001; Kaufman, 2003; Adam et al., 2018). GATA-3 expression was not different between control and $Egfr^{\Delta ep}$ mice (Figure 5A). However, LEF1 was only found to be expressed in IRS cells of $Egfr^{\Delta ep}$ mice, but not in hair shaft cells (Figure 5B). Staining for trichohyalin AE15, which is present in differentiated IRS and medulla, revealed lack of properly differentiated medulla cells in $Egfr^{\Delta ep}$ mice (Figure 5C).

Based on our results, we propose that EGFR signaling affects spatial layering during HF growth and differentiation (Figures 5D and 5E). First, EGFR promotes cell proliferation and ensures DNA integrity in highly proliferative epidermal compartments, such as IFE, ORS, and matrix. Upon loss of EGFR in those compartments, accumulation of DNA damage mediates TP53-dependent apoptosis (Figure 5D). Second, EGFR controls hair-layer-specific transcription factor expression to regulate epithelial hair layer specification and differentiation. EGFR deficiency leads to absence of proper differentiation cues for hair shaft cells, resulting in TP53-independent loss of the medulla layer (Figure 5E).

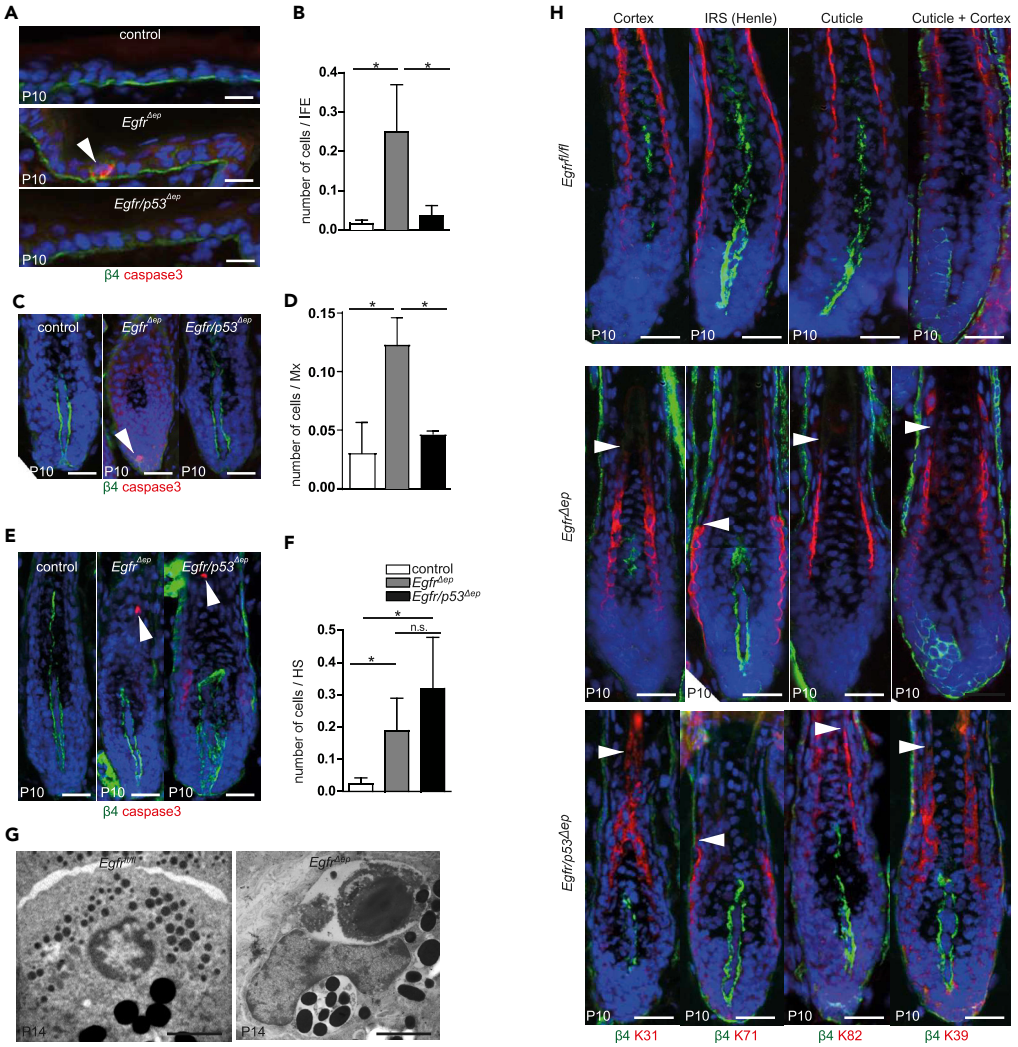

Figure 4. Apoptosis in IFE and Matrix Is TP53 Dependent, whereas Loss of Inner Hair Layers Is TP53 Independent

(A) Immunofluorescence staining for ITGB4 (green), activated caspase 3 (red) and nuclei (blue) from control, $Egfr^{\Delta ep}$, and $Egfr/p53^{\Delta ep}$ mice at P10, showing IFE. Arrow highlights an apoptotic cell.

(B) Quantification of the number of activated caspase 3^{+} IFE cells from control, $Egfr^{\Delta ep}$, and $Egfr/p53^{\Delta ep}$ mice at P10. Bars show analysis of 10 microscopic fields per mouse from n = 3 mice per genotype. Data are represented as mean ± SD. p values less than 0.05 were considered significant, with *p < 0.05 as determined by Kruskal-Wallis test.

(C) Immunofluorescence staining for ITGB4 Integrin (green), activated caspase 3 (red), and nuclei (blue) from control, $Egfr^{\Delta ep}$, and $Egfr/p53^{\Delta ep}$ mice at P10, showing HF matrix (Mx). Arrow highlights an apoptotic cell.

(D) Quantification of the number of activated caspase 3^{+} matrix cells from control, $Egfr^{\Delta ep}$, and $Egfr/p53^{\Delta ep}$ mice at P10. Bars show analysis of 20–30 hair follicles per mouse from n = 3 mice per genotype. Data are represented as mean ± SD. p values less than 0.05 were considered significant, with *p < 0.05 as determined by Kruskal-Wallis test.

(E) Immunofluorescence staining for ITGB4 (green), activated caspase 3 (red), and nuclei (blue) from control, $Egfr^{\Delta ep}$, and $Egfr/p53^{\Delta ep}$ mice at P10, showing hair shaft (HS). Arrows highlight apoptotic cells.

(F) Quantification of the number of activated caspase 3^{+} hair shaft cells from control, $Egfr^{\Delta ep}$, and $Egfr/p53^{\Delta ep}$ mice at P10. Bars show analysis of 20–30 hair follicles per mouse from n = 3 mice per genotype. Data are represented as mean ± SD. p values less than 0.05 were considered significant, with *p < 0.05 as determined by Kruskal-Wallis test.

(G) Transmission electron microscopic image of medulla cells from P14 control and $Egfr^{\Delta ep}$ mice. Scale bars, 2 μm.

(H) Immunofluorescence staining for ITGB4 (green), cortex marker K31 (red), and nuclei (blue) from control, $Egfr^{\Delta ep}$, and $Egfr/p53^{\Delta ep}$ mice at P10 (far left). Immunofluorescence staining for ITGB4 (green), IRS (Henle layer) marker K71 (red), and nuclei (blue) from control, $Egfr^{\Delta ep}$, and $Egfr/p53^{\Delta ep}$ mice at P10 (middle left). Immunofluorescence staining for ITGB4

Figure 4. *Continued*
(green), cuticle marker K82 (red), and nuclei (blue) from control, $Egfr^{\Delta ep}$, and $Egfr/p53^{\Delta ep}$ mice at P10 (middle right). Immunofluorescence staining for ITGB4 (green), cuticle and cortex marker K39 (red), and nuclei (blue) from control, $Egfr^{\Delta ep}$, and $Egfr/p53^{\Delta ep}$ mice at P10 (far right). Arrows highlight disappearance of layers.
Scale bars, 20 μm unless otherwise stated. See also Figure S4.

Loss of EGFR in Adult HFSCs Results in Growth Delay

We next investigated whether EGFR also serves a growth-promoting function in adult HFSCs. Therefore, we first tested whether EGFR is expressed in adult HFSCs by applying fluorescently labeled epidermal growth factor to cell suspensions of adult (P45) wild-type mice after completion of the first hair cycle, when hair is in early telogen. We detected high EGFR expression in $CD34^+$ old and new bulge stem cells, intermediate expression in IFE, and no expression in $CD45^+$ hematopoietic cells using flow cytometric analysis (Figure S5A). These results were confirmed by EGFR stainings on back skin sections (Figure S5B). Furthermore, EGFR expression was detected within the matrix, the ORS and the IRS of anagen HFs (Figures S5C and S5D). During catagen, scattered EGFR expression was observed in the retracting HF (Figure S5E). These results suggest that EGFR signaling is required in adult HFSCs. Because it is not possible to investigate activation and growth of adult HFSCs in $Egfr^{\Delta ep}$ mice owing to HF degradation and progressive hair loss (Lichtenberger et al., 2013), we crossed $Egfr^{fl/fl}$ to $Lgr5Cre^{ERT2}GFP$ mice to delete the EGFR after completion of the first postnatal hair cycle (from P43-P47) in lower bulge and secondary hair germ (2°HG) HFSCs by tamoxifen injection ($EGFR^{\Delta LGR5-ERT2}$ mice, Figure S5F). $Egfr^{\Delta LGR5\text{-}ERT2}$ mice were monitored during progression of the second postnatal hair cycle until P88. EGFR deletion was confirmed by genomic DNA (Figure S5G) and by immunohistochemistry (IHC) analysis (Figure S5H). $Egfr^{\Delta LGR5\text{-}ERT2}$ mice exhibited delayed entry into the second hair cycle (Figure 6A), demonstrating that EGFR signaling is involved in HFSC activation and proliferation. This was further underlined by the finding that by the time of analysis most follicles of control mice had completed the second hair cycle and already returned to telogen, whereas the majority of HFs of $Egfr^{\Delta LGR5\text{-}ERT2}$ mice was still in anagen of the second cycle (Figure 6B). Importantly, $Egfr^{\Delta LGR5\text{-}ERT2}$ mice did not display an immune cell infiltrate (Figure 6C), emphasizing that the growth delay observed in $Egfr^{\Delta LGR5\text{-}ERT2}$ mice is solely due to cell-autonomous defects in HFSCs.

To identify molecules deregulated in adult HFSCs upon loss of EGFR, we performed flow cytometric cell sorting of $LGR5^+$ cells from P88 control and $Egfr^{\Delta LGR5\text{-}ERT2}$ mice and subjected them to RNA-seq (Figures S5I and S5J). We found 145 genes to be significantly differentially expressed between $LGR5^+$ cells derived from control and $Egfr^{\Delta LGR5\text{-}ERT2}$ mice (Figures 6D and 6E, Table S2A). Among the differentially expressed genes, we found genes encoding for structural proteins that were deregulated in our dataset obtained from P2 $Egfr^{\Delta ep}$ mice such as *Gjb4* and *Klk7* and also genes encoding for signaling and growth molecules such as *Wnt3a* or *Bmp7* indicating that lack of EGFR signaling in $LGR5^+$ HFSCs broadly shifts the balance of molecules regulating HFSC behavior. Overall, affected genes show enrichment for GO terms such as "cellular response to chemical stimulus," "tissue development," "molting cycle," or "growth" (Figures 6F and 6G, Tables S2B and S2C). Thus loss of EGFR negatively alters the susceptibility of HFSCs to respond to activating cues (Figure 6H).

Investigation of receptor and ligand expression in control $LGR5^+$ HFSCs revealed that similar to P2 IFE and ORS, these cells highly express *Egfr*, *Erbb2*, and *Erbb3*, but not *Erbb4*. Moreover, $LGR5^+$ HFSCs display low expression of the ligands *Tgfα*, *Epgn*, and *Hb-egf*, whereas all other ligands are not expressed (Figure S5K).

Furthermore, exons or junction sites of more than 300 genes were affected by alternative splicing alterations in $LGR5^+$ cells of $Lgr5^+$ $Egfr^{\Delta LGR5\text{-}ERT2}$ mice, enriching for GO terms associated with cell stimulation and intracellular metabolic processes (Figure S5L, Table S2D). Notably, we detected a substantial overlap of alternative transcripts from 213 genes (10.3%) between P2 IFE + ORS and P88 $LGR5^+$ cells (Figure S5M, Table S2E), leading to the assumption that EGFR has some identical targets in distinct epidermal compartments at different time points, as well as a variety of specific targets depending on epidermal cell identity and age. Shared target genes display significant enrichment for GO terms such as "organelle," "intracellular signal transduction," and "cell cycle" (Figure S5N, Table S2F), further underlining that EGFR is required for proliferation and proper orchestration of molecules and pathways involved in both HF development and adult HFSC activation and new HF growth.

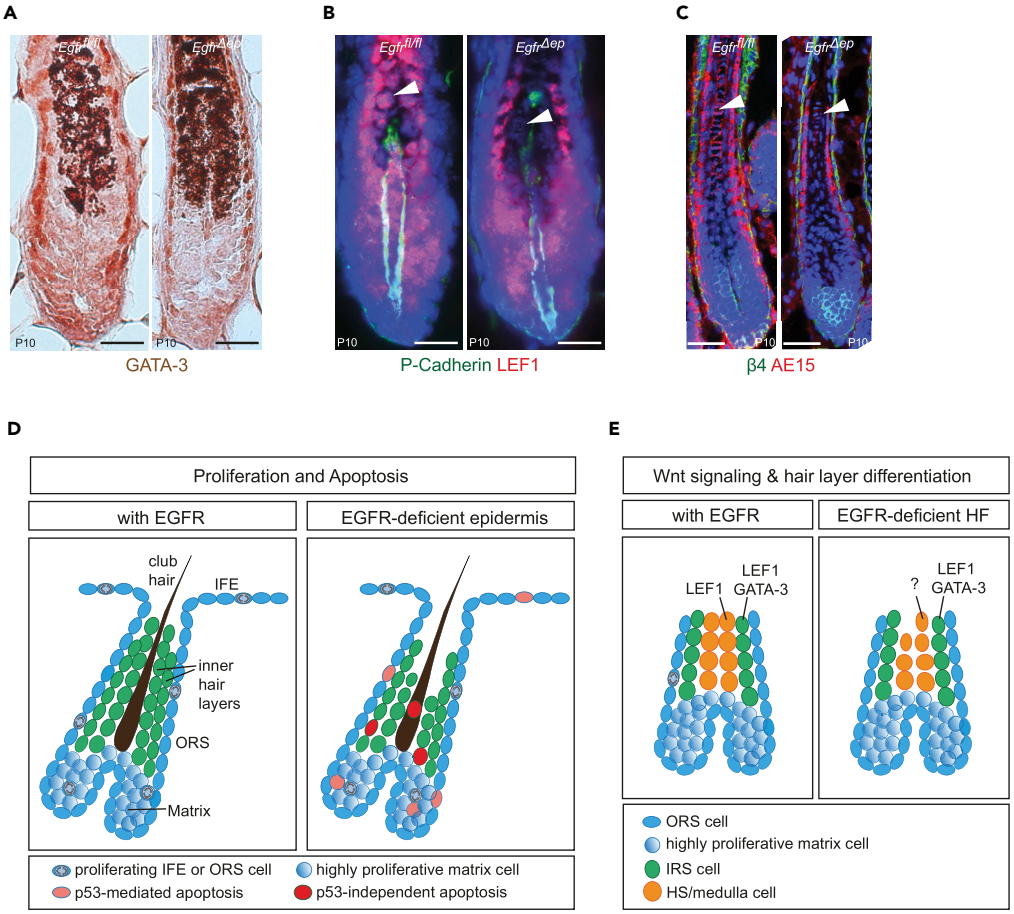

Figure 5. EGFR Controls Hair Lineage Transcription Factor Expression

(A) IHC staining of GATA-3 from P10 control and $Egfr^{\Delta ep}$ mice.

(B) Immunofluorescence staining for P-Cadherin (green), LEF1 (red), and nuclei (blue) from P10 control and $Egfr^{\Delta ep}$ mice. Arrowheads point to hair shaft cells.

(C) Immunofluorescence staining for ITGB4 (green), IRS and medulla marker AE15 (red), and nuclei (blue) from control and $Egfr^{\Delta ep}$ mice at P10. Arrowheads point on medulla cells.

(D) Model summarizing TP53-dependent mechanisms of cell death in IFE, ORS, and medulla during the growth phase of HF morphogenesis in $Egfr^{\Delta ep}$ mice.

(E) Model summarizing TP53-independent effects of EGFR deficiency in epithelial hair lineages.

Scale bars, 20 μm unless otherwise stated.

DISCUSSION

Our study demonstrates that the phenotype of EGFR-deficient skin is multifactorial, displaying alterations in expression of structural proteins, DNA integrity and DNA damage, proliferation, and apoptosis, but not stem cell identity genes. Lack of EGFR in newborn skin reduces proliferation in ORS and also in IFE keratinocytes. Analysis of RNA-seq data and subsequent histological analysis demonstrate reduced ERK activation and loss of expression of the ERK downstream target *Egr1* (Mayer et al., 2009; Tarcic et al., 2011) in EGFR-deficient ORS. In various studies on cancer cells and in mouse models of ERBB2 overexpression a prominent function of EGFR signaling in promoting keratinocyte proliferation via ERK phosphorylation has been shown (Lichtenberger et al., 2010) (Bol et al., 1998; Xie et al., 1999; Kiguchi et al., 2000). The proliferation-promoting function of EGFR was mainly assessed in a hyperproliferative context of tumor cells, whereas only little information is available in the framework of epidermal morphogenesis and homeostasis. Albeit a reduction of proliferating keratinocytes was shown for the IFE of $Egfr^{-/-}$ mice (Hansen et al., 1997), this was never formally shown for the ORS. Importantly, previous studies investigating adult EGFR-deficient mice could not show changes in pERK by using *in vitro* assays (Nagao et al., 2012) or *in vivo* analysis (Wolf et al., 2016). The absence of effects on pERK levels might be due to assessment of fully developed adult

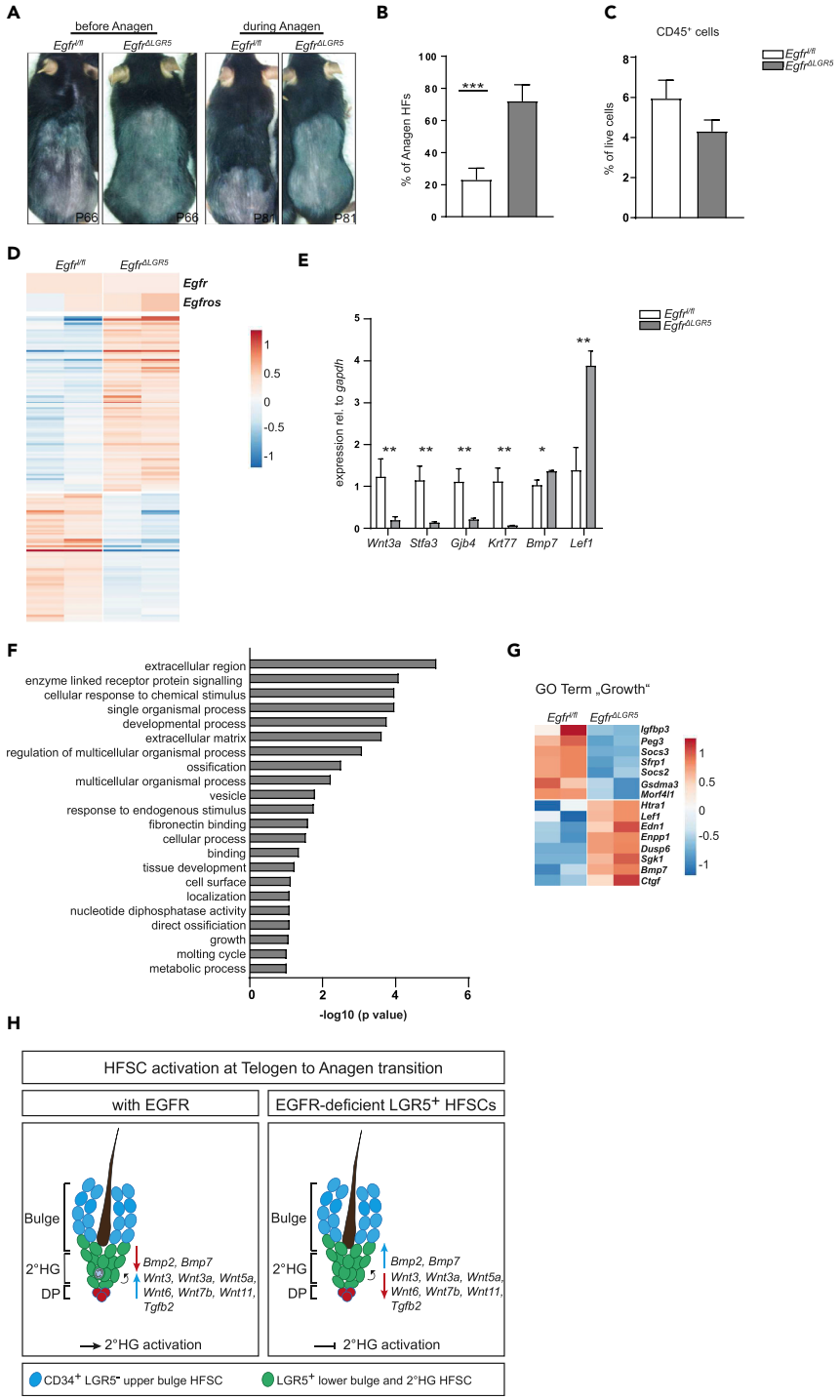

Figure 6. Loss of EGFR in Adult HFSCs Results in Growth Delay

(A) Photographs of shaved back skin from control and *Egfr*$^{\Delta LGR5}$ mice before and during anagen of second hair cycle.

(B) Quantification of percentage of anagen HFs in mice of indicated genotypes at P88. Bars show analysis of 10 hair follicles per mouse from n = 7–8 mice per genotype. Data are represented as mean ± SD. p values less than 0.05 were considered significant, with ***p < 0.001 as determined by Student's t test.

(C) Quantification of CD45$^+$ cells in P88 control and *Egfr*$^{\Delta LGR5}$ mice. Bars show analysis of n = 3–5 mice per genotype. Data are represented as mean ± SD. p values less than 0.05 were considered significant. The data sets do not show staticstical significance as determined by Student's t test.

Figure 6. *Continued*

(D) Heatmap of significantly deregulated genes between P88 control and $Egfr^{\Delta LGR5}$ mice. Each column represents one mouse.

(E) Graphical representation of qRT-PCR validation of randomly selected target genes from $LGR5^{+}$ cells of P88 control and $Egfr^{\Delta LGR5}$ mice. Bars show analysis of n = 4 mice per genotype. Data are represented as mean ± SD. p values less than 0.05 were considered significant, with *$p < 0.05$, **$p < 0.01$ as determined by Student's t test.

(F) Bar diagram of GO terms of significantly deregulated genes.

(G) Heatmap of deregulated genes belonging to GO Term "growth." Each column represents one mouse.

(H) Model depicting the effects of EGFR in adult HFSCs.

See also Figure S5 and Tables S2A–S2F.

murine skin, and not neonatal mice, undergoing epidermal morphogenesis. In addition, many other pathways have been shown to induce ERK phosphorylation in keratinocytes. Thus our data provide new insight into a growth-promoting function of EGFR in the developing ORS.

We assessed the specification of committed HFSC populations during early HF development by using markers LHX2, NFATc1, and NPNT. All factors were equally expressed and localized in control and $Egfr^{\Delta ep}$ mice. Among the group of epidermal structural genes displaying differential gene expression in our RNA-seq dataset were factors that each alone can result in severe epidermal or hair alterations: mutations in *Flg* are known to be involved in the development of atopic dermatitis (Tholen et al., 2016), mutations in *Spink5* are reported to cause Netherton syndrome (Raghunath et al., 2004), and mutations in *Gjb4* are associated with erythrokeratodermia variabilis (Richard et al., 2003). These findings demonstrate that one critical role of EGFR signaling is transcriptional regulation of structural genes directly involved in epidermal differentiation.

We identified centrosome assembly and function as a novel downstream process of EGFR signaling by our expression and alternative splicing analysis. IFE keratinocytes lacking EGFR display centrosome amplifications. Functional consequences of abnormal centrosome numbers due to a disbalance in centrosomal proteins were previously shown to correlate with genome instability (Vitre and Cleveland, 2012; Nam et al., 2015). Importantly, defects in centrosome or mitotic spindle assembly leading to the generation of multiple nuclei are partially causative for the rare disease trichothiodystrophy (Nakabayashi et al., 2005; Zhang et al., 2007), which affects DNA repair and hair structure.

Generally, genome instability and nuclear fragmentation are accompanied by DNA damage. In the epidermis, centrosome amplifications result in impaired mitosis and TP53-mediated cell death (Kulukian et al., 2015). In our datasets, we find transcriptional upregulation of genes associated with cellular response to DNA damage in $Egfr^{\Delta ep}$ mice: TP53 apoptosis effector *Perp* is known as an apoptosis-associated target of TP53, involved in its stabilization (Attardi et al., 2000; Davies et al., 2011), and *Hmgn2* was reported to facilitate chromatin accessibility for DNA repair machinery (Subramanian et al., 2009). So far, cross talk between EGFR and TP53 signaling was only shown *in vitro* (Kryeziu et al., 2013). Importantly, our data for the first time provide *in vivo* evidence for a role of EGFR signaling in prevention of DNA damage in proliferating cells and for susceptibility of epidermal cells to TP53-mediated apoptosis upon loss of EGFR. Despite the DNA-damage-induced apoptosis in proliferative keratinocyte compartments, we detect TP53-independent cell loss in differentiated epithelial hair layers comprising the hair shaft. Suprabasal-transit-amplifying cells, which give rise to those innermost hair layers, display a requirement for EGFR signaling to induce correct transcription factor expression of the lineage diversification factor *Lef1*. During morphogenesis, LEF1 protein is not detectable in hair shaft cells of EGFR-deficient epidermis, thus presumably reducing the expression of hair-shaft-specific genes. These defects ultimately lead to loss of hair shaft cells, hair structure alteration, and hair malformation.

Limitation of the Study

We are formally not able to discriminate between a cell-autonomous function of EGFR in epithelial hair lineage differentiation, or a secondary effect on hair shaft differentiation following absence of EGFR in all epithelial skin lineages. To date, there are no-hair shaft-specific Cre lines available that would allow detailed investigation of the effects of *Egfr* deletion in these particular hair lineages.

METHODS

All methods can be found in the accompanying Transparent Methods supplemental file.

SUPPLEMENTAL INFORMATION

Supplemental Information can be found online at https://doi.org/10.1016/j.isci.2019.04.018.

ACKNOWLEDGMENTS

We thank the Core Facility "Flow Cytometry" of the Medical University of Vienna for help with FACS sorting; and the Core Facility "Genomics" of the Medical University of Vienna for performance of RNA quality control, library preparation, and RNA-seq; as well as Margit Pavelka from the Medical University of Vienna and Daniela Gruber from the University of Vienna for help with Transmission Electron Microscopy (TEM) sample preparation. TEM imaging was performed at the Core Facility "Cell Imaging and Ultrastructure Research" at the University of Vienna. Moreover, we thank Christine Tuppy for assistance in primary keratinocyte culture and are grateful to Martina Hammer and the staff of the Department of Biomedical Research for maintaining our mouse colonies. We thank Khalil Kass Youssef for assistance with histology, Caroline Stremnitzer for critical reading of the manuscript, and Florian Pauler for assistance in R data processing. This work was supported by the Austrian Science Fund (FWF) grants FWF-DK W1212 and the Austrian Federal Government's GEN-AU program "Austromouse" (GZ 200.147/1-VI/1a/2006 and 820966). M.S.'s research is funded by the European Research Council (ERC) under the Horizon 2020 research and innovation program (grant agreement ERC-2015-AdG 694883), the EU H2020 MSCA ITN-766241, and the Vienna Science and Technology Fund (WWTF, grant agreement LS16-025).

AUTHOR CONTRIBUTIONS

N.A. designed and performed most of the experiments. P.A.S. provided intellectual and experimental input. G.H. analyzed RNA-seq data. M.H. provided intellectual input. B.M.L. performed hair staging analysis. B.C. performed qRT-PCR. T.B.-G. helped with TEM. C.B. provided intellectual input as well as laboratory space and reagents. M.S. supervised the whole project. N.A., M.H., and M.S. wrote the manuscript.

DECLARATION OF INTERESTS

The authors declare no conflicts of interest.

Received: January 28, 2019
Revised: March 15, 2019
Accepted: April 15, 2019
Published: May 31, 2019

REFERENCES

Adam, R.C., Yang, H., Ge, Y., Lien, W.H., Wang, P., Zhao, Y., Polak, L., Levorse, J., Baksh, S.C., Zheng, D., et al. (2018). Temporal layering of signaling effectors drives chromatin remodeling during hair follicle stem cell lineage progression. Cell Stem Cell *22*, 398–413.e7.

Attardi, L.D., Reczek, E.E., Cosmas, C., Demicco, E.G., McCurrach, M.E., Lowe, S.W., and Jacks, T. (2000). PERP, an apoptosis-associated target of p53, is a novel member of the PMP-22/gas3 family. Genes Dev. *14*, 704–718.

Bichsel, K.J., Hammiller, B., Trempus, C.S., Li, Y., and Hansen, L.A. (2016). The epidermal growth factor receptor decreases Stathmin 1 and triggers catagen entry in the mouse. Exp. Dermatol. *25*, 275–281.

Blanpain, C., and Fuchs, E. (2009). Epidermal homeostasis: a balancing act of stem cells in the skin. Nat. Rev. Mol. Cell Biol. *10*, 207–217.

Bol, D., Kiguchi, K., Beltran, L., Rupp, T., Moats, S., Gimenez-Conti, I., Jorcano, J., and DiGiovanni, J. (1998). Severe follicular hyperplasia and spontaneous papilloma formation in transgenic mice expressing the neu oncogene under the control of the bovine keratin 5 promoter. Mol. Carcinog. *21*, 2–12.

Crew, F.A.E. (1933). Waved - an autosomal recessive coat form character in the mouse. J. Genet. *27*, 95–96.

Dahlhoff, M., Frances, D., Kloepper, J.E., Paus, R., Schafer, M., Niemann, C., and Schneider, M.R. (2014). Overexpression of epigen during embryonic development induces reversible, epidermal growth factor receptor-dependent sebaceous gland hyperplasia. Mol. Cell. Biol. *34*, 3086–3095.

DasGupta, R., and Fuchs, E. (1999). Multiple roles for activated LEF/TCF transcription complexes during hair follicle development and differentiation. Development *126*, 4557–4568.

Davies, L., Spiller, D., White, M.R., Grierson, I., and Paraoan, L. (2011). PERP expression stabilizes active p53 via modulation of p53-MDM2 interaction in uveal melanoma cells. Cell Death Dis. *2*, e136.

Devenport, D., and Fuchs, E. (2008). Planar polarization in embryonic epidermis orchestrates global asymmetric morphogenesis of hair follicles. Nat. Cell Biol. *10*, 1257–1268.

Folgueras, A.R., Guo, X., Pasolli, H.A., Stokes, N., Polak, L., Zheng, D., and Fuchs, E. (2013). Architectural niche organization by LHX2 is linked to hair follicle stem cell function. Cell Stem Cell *13*, 314–327.

Franzke, C.W., Cobzaru, C., Triantafyllopoulou, A., Loffek, S., Horiuchi, K., Threadgill, D.W., Kurz, T., van Rooijen, N., Bruckner-Tuderman, L., and Blobel, C.P. (2012). Epidermal ADAM17 maintains the skin barrier by regulating EGFR ligand-dependent terminal keratinocyte differentiation. J. Exp. Med. *209*, 1105–1119.

Fujiwara, H., Ferreira, M., Donati, G., Marciano, D.K., Linton, J.M., Sato, Y., Hartner, A., Sekiguchi, K., Reichardt, L.F., and Watt, F.M. (2011). The basement membrane of hair follicle stem cells is a muscle cell niche. Cell *144*, 577–589.

Graveley, B.R., and Maniatis, T. (1998). Arginine/serine-rich domains of SR proteins can function as activators of pre-mRNA splicing. Mol. Cell *1*, 765–771.

Hansen, L.A., Alexander, N., Hogan, M.E., Sundberg, J.P., Dlugosz, A., Threadgill, D.W., Magnuson, T., and Yuspa, S.H. (1997). Genetically null mice reveal a central role for epidermal growth factor receptor in the differentiation of the

hair follicle and normal hair development. Am. J. Pathol. *150*, 1959–1975.

Hartley, S.W., and Mullikin, J.C. (2016). Detection and visualization of differential splicing in RNA-Seq data with JunctionSeq. Nucleic Acids Res. *44*, e127.

Horsley, V., Aliprantis, A.O., Polak, L., Glimcher, L.H., and Fuchs, E. (2008). NFATc1 balances quiescence and proliferation of skin stem cells. Cell *132*, 299–310.

Hsu, Y.-C., Li, L., and Fuchs, E. (2014). Emerging interactions between skin stem cells and their niches. Nat. Med. *20*, 847–856.

Huelsken, J., Vogel, R., Erdmann, B., Cotsarelis, G., and Birchmeier, W. (2001). β-Catenin controls hair follicle morphogenesis and stem cell differentiation in the skin. Cell *105*, 533–545.

Jaks, V., Barker, N., Kasper, M., van Es, J.H., Snippert, H.J., Clevers, H., and Toftgård, R. (2008). Lgr5 marks cycling, yet long-lived, hair follicle stem cells. Nat. Genet. *40*, 1291–1299.

Kaufman, C.K. (2003). GATA-3: an unexpected regulator of cell lineage determination in skin. Genes Dev. *17*, 2108–2122.

Kiguchi, K., Bol, D., Carbajal, S., Beltran, L., Moats, S., Chan, K., Jorcano, J., and DiGiovanni, J. (2000). Constitutive expression of erbB2 in epidermis of transgenic mice results in epidermal hyperproliferation and spontaneous skin tumor development. Oncogene *19*, 4243–4254.

Kryeziu, K., Jungwirth, U., Hoda, M.A., Ferk, F., Knasmuller, S., Karnthaler-Benbakka, C., Kowol, C.R., Berger, W., and Heffeter, P. (2013). Synergistic anticancer activity of arsenic trioxide with Erlotinib is based on inhibition of EGFR-mediated DNA double-strand break repair. Mol. Cancer Ther. *12*, 1073–1084.

Kulukian, A., Holland, A.J., Vitre, B., Naik, S., Cleveland, D.W., and Fuchs, E. (2015). Epidermal development, growth control, and homeostasis in the face of centrosome amplification. Proc. Natl. Acad. Sci. U S A *112*, E6311–E6320.

Lee, J., Kumagai, A., and Dunphy, W.G. (2003). Claspin, a Chk1-regulatory protein, monitors DNA replication on chromatin independently of RPA, ATR, and Rad17. Mol. Cell *11*, 329–340.

Li, Y., Stoll, S.W., Sekhon, S., Talsma, C., Camhi, M.I., Jones, J.L., Lambert, S., Marley, H., Rittie, L., Grachtchouk, M., et al. (2016). Transgenic expression of human amphiregulin in mouse skin: inflammatory epidermal hyperplasia and enlarged sebaceous glands. Exp. Dermatol. *25*, 187–193.

Lichtenberger, B.M., Gerber, P.A., Holcmann, M., Buhren, B.A., Amberg, N., Smolle, V., Schrumpf, H., Boelke, E., Ansari, P., Mackenzie, C., et al. (2013). Epidermal EGFR controls cutaneous host defense and prevents inflammation. Sci. Transl. Med. *5*, 199ra111.

Lichtenberger, B.M., Tan, P.K., Niederleithner, H., Ferrara, N., Petzelbauer, P., and Sibilia, M. (2010). Autocrine VEGF signaling synergizes with EGFR in tumor cells to promote epithelial cancer development. Cell *140*, 268–279.

Luetteke, N.C., Phillips, H.K., Qiu, T.H., Copeland, N.G., Earp, H.S., Jenkins, N.A., and Lee, D.C. (1994). The mouse waved-2 phenotype results from a point mutation in the EGF receptor tyrosine kinase. Genes Dev. *8*, 399–413.

Luetteke, N.C., Qiu, T.H., Peiffer, R.L., Oliver, P., Smithies, O., and Lee, D.C. (1993). TGFα deficiency results in hair follicle and eye abnormalities in targeted and waved-1 mice. Cell *73*, 263–278.

Mascia, F., Lam, G., Keith, C., Garber, C., Steinberg, S.M., Kohn, E., and Yuspa, S.H. (2013). Genetic ablation of epidermal EGFR reveals the dynamic origin of adverse effects of anti-EGFR therapy. Sci. Transl. Med. *5*, 199ra110.

Mayer, S.I., Rossler, O.G., Endo, T., Charnay, P., and Thiel, G. (2009). Epidermal-growth-factor-induced proliferation of astrocytes requires Egr transcription factors. J. Cell Sci. *122*, 3340–3350.

Merrill, B.J. (2001). Tcf3 and Lef1 regulate lineage differentiation of multipotent stem cells in skin. Genes Dev. *15*, 1688–1705.

Miettinen, P.J., Berger, J.E., Meneses, J., Phung, Y., Pedersen, R.A., Werb, Z., and Derynck, R. (1995). Epithelial immaturity and multiorgan failure in mice lacking epidermal growth factor receptor. Nature *376*, 337–341.

Muller-Rover, S., Tokura, Y., Welker, P., Furukawa, F., Wakita, H., Takigawa, M., and Paus, R. (1999). E- and P-cadherin expression during murine hair follicle morphogenesis and cycling. Exp. Dermatol. *8*, 237–246.

Murillas, R., Larcher, F., Conti, C.J., Santos, M., Ullrich, A., and Jorcano, J.L. (1995). Expression of a dominant negative mutant of epidermal growth factor receptor in the epidermis of transgenic mice elicits striking alterations in hair follicle development and skin structure. EMBO J. *14*, 5216–5223.

Nagao, K., Kobayashi, T., Ohyama, M., Akiyama, H., Horiuchi, K., and Amagai, M. (2012). Brief report: requirement of TACE/ADAM17 for hair follicle bulge niche establishment. Stem Cells *30*, 1781–1785.

Nakabayashi, K., Amann, D., Ren, Y., Saarialho-Kere, U., Avidan, N., Gentles, S., MacDonald, J.R., Puffenberger, E.G., Christiano, A.M., Martinez-Mir, A., et al. (2005). Identification of C7orf11 (TTDN1) gene mutations and genetic heterogeneity in nonphotosensitive trichothiodystrophy. Am. J. Hum. Genet. *76*, 510–516.

Nam, H.J., Naylor, R.M., and van Deursen, J.M. (2015). Centrosome dynamics as a source of chromosomal instability. Trends Cell Biol. *25*, 65–73.

Natarajan, A., Wagner, B., and Sibilia, M. (2007). The EGF receptor is required for efficient liver regeneration. Proc. Natl. Acad. Sci. U S A *104*, 17081–17086.

Raghunath, M., Tontsidou, L., Oji, V., Aufenvenne, K., Schurmeyer-Horst, F., Jayakumar, A., Stander, H., Smolle, J., Clayman, G.L., and Traupe, H. (2004). SPINK5 and Netherton syndrome: novel mutations, demonstration of missing LEKTI, and differential expression of transglutaminases. J. Invest. Dermatol. *123*, 474–483.

Richard, G., Brown, N., Rouan, F., Van der Schroeff, J.G., Bijlsma, E., Eichenfield, L.F., Sybert, V.P., Greer, K.E., Hogan, P., Campanelli, C., et al. (2003). Genetic heterogeneity in erythrokeratodermia variabilis: novel mutations in the connexin gene GJB4 (Cx30.3) and genotype-phenotype correlations. J. Invest. Dermatol. *120*, 601–609.

Sibilia, M., Wagner, B., Hoebertz, A., Elliott, C., Marino, S., Jochum, W., and Wagner, E.F. (2003). Mice humanised for the EGF receptor display hypomorphic phenotypes in skin, bone and heart. Development *130*, 4515–4525.

Sibilia, M., and Wagner, E. (1995). Strain-dependent epithelial defects in mice lacking the EGF receptor. Science *269*, 234–238.

Subramanian, M., Gonzalez, R.W., Patil, H., Ueda, T., Lim, J.H., Kraemer, K.H., Bustin, M., and Bergel, M. (2009). The nucleosome-binding protein HMGN2 modulates global genome repair. FEBS J. *276*, 6646–6657.

Szebenyi, G., Hall, B., Yu, R., Hashim, A.I., and Kramer, H. (2007). Hook2 localizes to the centrosome, binds directly to centriolin/CEP110 and contributes to centrosomal function. Traffic *8*, 32–46.

Tarcic, G., Avraham, R., Pines, G., Amit, I., Shay, T., Lu, Y., Zwang, Y., Katz, M., Ben-Chetrit, N., Jacob-Hirsch, J., et al. (2011). EGR1 and the ERK-ERF axis drive mammary cell migration in response to EGF. FASEB J. *26*, 1582–1592.

Tholen, S., Wolf, C., Mayer, B., Knopf, J.D., Loffek, S., Qian, Y., Kizhakkedathu, J.N., Biniossek, M.L., Franzke, C.W., and Schilling, O. (2016). Skin barrier defects caused by keratinocyte-specific deletion of ADAM17 or EGFR are based on highly similar proteome and degradome alterations. J. Proteome Res. *15*, 1402–1417.

Threadgill, D.W., Dlugosz, A.A., Hansen, L.A., Tennenbaum, T., Lichti, U., Yee, D., LaMantia, C., Mourton, T., Herrup, K., and Harris, R.C. (1995). Targeted disruption of mouse EGF receptor: effect of genetic background on mutant phenotype. Science *269*, 230–234.

Tumbar, T. (2012). Ontogeny and homeostasis of adult epithelial skin stem cells. Stem Cell Rev. *8*, 561–576.

Vitre, B.D., and Cleveland, D.W. (2012). Centrosomes, chromosome instability (CIN) and aneuploidy. Curr. Opin. Cell Biol. *24*, 809–815.

Wolf, C., Qian, Y., Brooke, M.A., Kelsell, D.P., and Franzke, C.W. (2016). ADAM17/EGFR axis promotes transglutaminase-dependent skin barrier formation through phospholipase C gamma1 and protein kinase C pathways. Sci. Rep. *6*, 39780.

Xie, W., Chow, L.T., Paterson, A.J., Chin, E., and Kudlow, J.E. (1999). Conditional expression of the ErbB2 oncogene elicits reversible hyperplasia in stratified epithelia and up-regulation of TGFalpha expression in transgenic mice. Oncogene *18*, 3593–3607.

Zhang, Y., Tian, Y., Chen, Q., Chen, D., Zhai, Z., and Shu, H.B. (2007). TTDN1 is a Plk1-interacting protein involved in maintenance of cell cycle integrity. Cell. Mol. Life Sci. *64*, 632–640.

ISCI, Volume *15*

Supplemental Information

EGFR Controls Hair Shaft Differentiation in a p53-Independent Manner

Nicole Amberg, Panagiota A. Sotiropoulou, Gerwin Heller, Beate M. Lichtenberger, Martin Holcmann, Bahar Camurdanoglu, Temenuschka Baykuscheva-Gentscheva, Cedric Blanpain, and Maria Sibilia

Fig. S1, Amberg et al

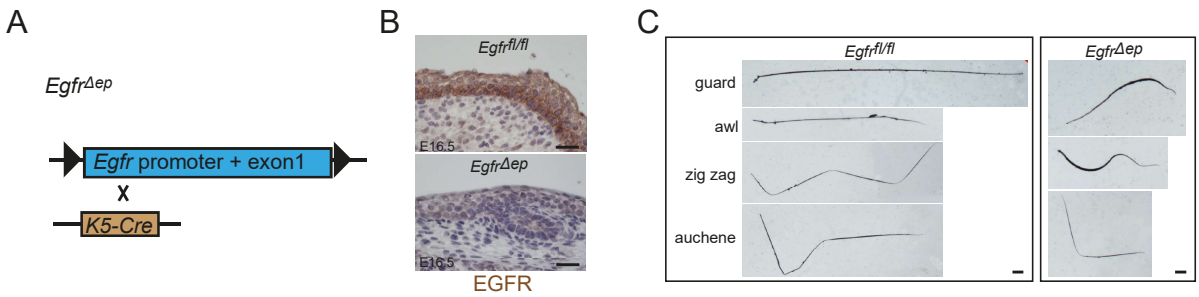

Figure S1. Loss of EGFR results in hair alterations. Related to Figure 1

(A) Schematic picture of *Egfr*$^{\Delta ep}$ mice.

(B) Immunohistochemistry staining of EGFR on sections of an E16.5 control and *Egfr*$^{\Delta ep}$ mouse.

(C) Brightfield images of plucked hair from P22 control and *Egfr*$^{\Delta ep}$ mice.

Scale bars 20μm unless otherwise stated.

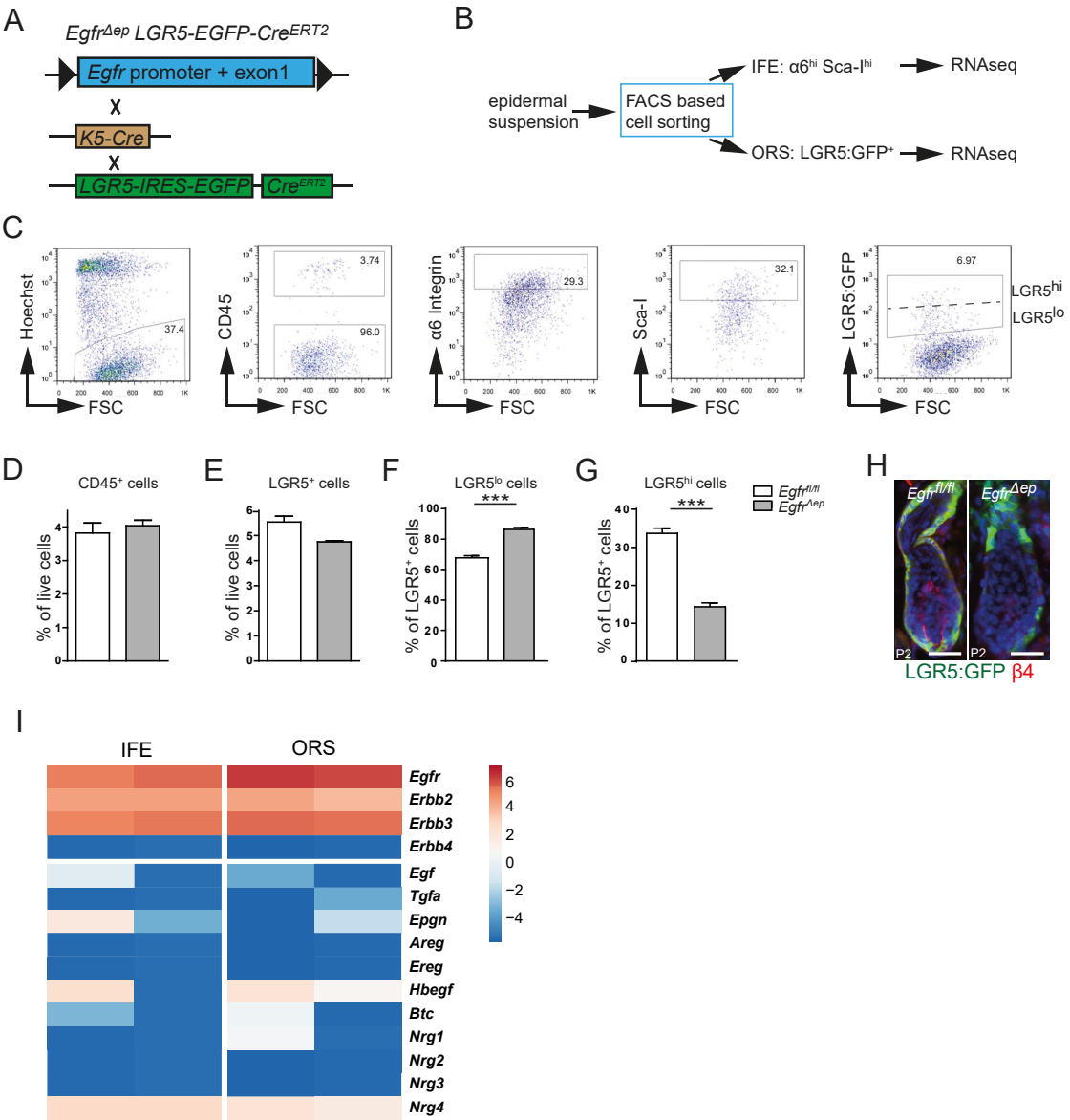
A
Egfr^Δep LGR5-EGFP-CreERT2
Egfr promoter + exon1
X
K5-Cre
X
LGR5-IRES-EGFP
CreERT2
B
epidermal suspension
FACS based cell sorting
IFE: α6hi Sca-Ihi
RNAseq
ORS: LGR5:GFP+
RNAseq
C
Hoechst
FSC
37.4
CD45
3.74
96.0
α6 Integrin
29.3
Sca-I
32.1
LGR5:GFP
6.97
LGR5hi
LGR5lo
D
CD45+ cells
% of live cells
E
LGR5+ cells
% of live cells
F
LGR5lo cells
***
% of LGR5+ cells
G
LGR5hi cells
***
% of LGR5+ cells
Egfrfl/fl
EgfrΔep
H
Egfrfl/fl
EgfrΔep
P2
P2
LGR5:GFP β4
I
IFE
ORS
Egfr
Erbb2
Erbb3
Erbb4
Egf
Tgfa
Epgn
Areg
Ereg
Hbegf
Btc
Nrg1
Nrg2
Nrg3
Nrg4
6
4
2
0
−2
−4

Figure S2. Flow cytometric analysis of newborn mouse skin. Related to Figure 2

(A) Schematic picture of *Egfr*$^{\Delta ep}$ *LGR5-Cre*^{ERT2}*GFP* mice.

(B) Schematic overview of work flow for RNAseq.

(C) FACS gating strategy for cell sorting of IFE and ORS cells from P2 control and *Egfr*$^{\Delta ep}$ *LGR5-Cre*^{ERT2}*GFP* mice.

(D) Quantification of CD45^{+} cells, (E) all LGR5:EGFP^{+} cells, (F) LGR5:EGFP^{lo} cells, and (G) LGR5:EGFP^{hi} cells as from FACS analysis of epidermal cell suspensions of P2 control and *Egfr*$^{\Delta ep}$ *LGR5-Cre*^{ERT2}*GFP* mice. Bars show data from n = 4-5 mice per genotype. Statistical significance was determined by Student's t-test with $p < 0.5$ *, $p < 0.01$ **, $p < 0.005$ ***.

(H) Immunofluorescence staining for GFP (green), ITGB4 (red) and nuclei (blue) from P2 control and *Egfr*$^{\Delta ep}$ *LGR5-Cre*^{ERT2}*GFP* mice, showing HF.

(I) Heat map showing expression of *Erbb* receptors and their ligands in control samples from P2 IFE and P2 ORS. Each column represents one mouse.

Scale bars 20µm unless otherwise stated.

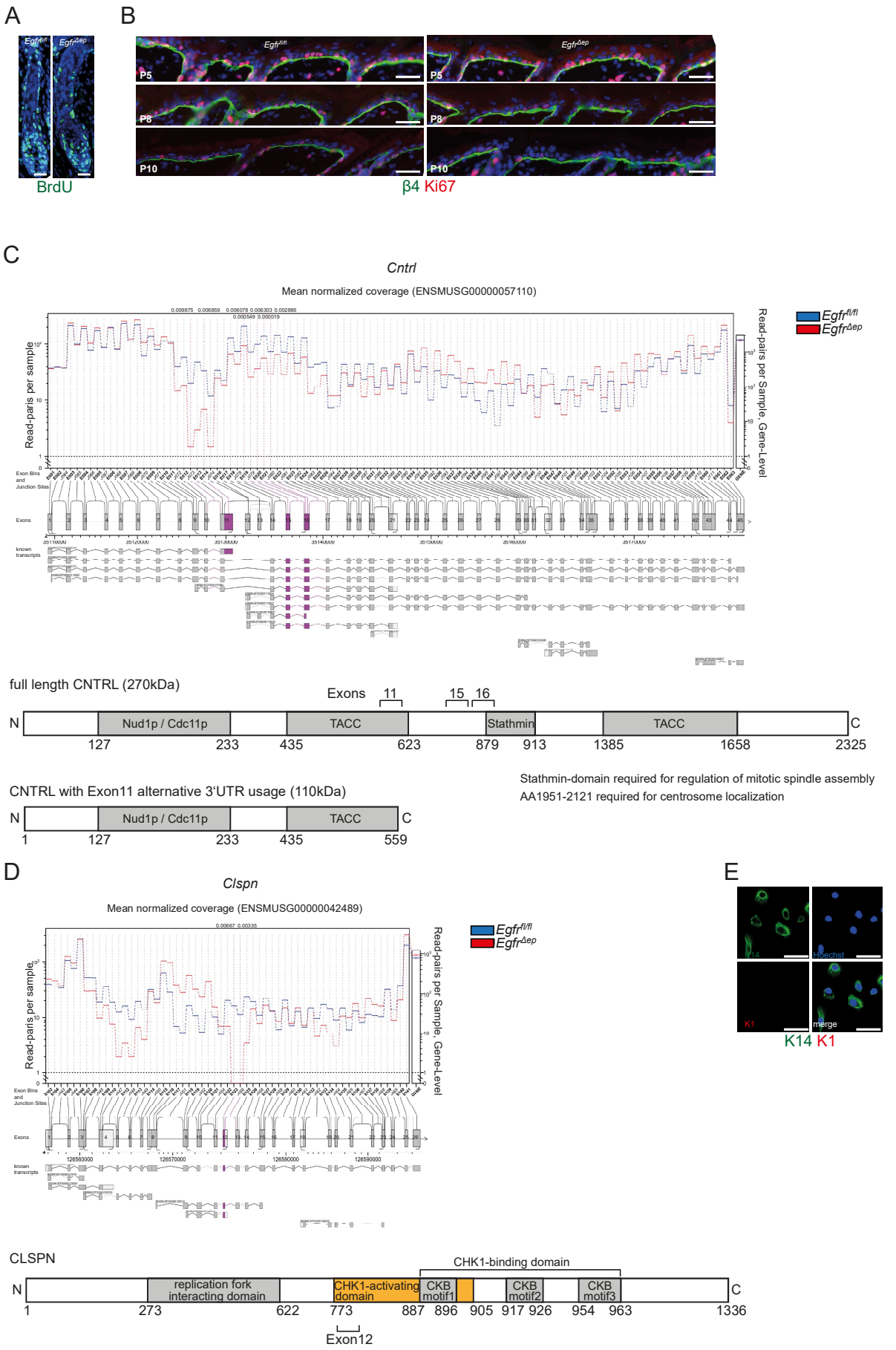
A
B
Egfr^fl/fl
Egfr^Δep
P5
P8
P10
BrdU
β4 Ki67
C
Cntrl
Mean normalized coverage (ENSMUSG00000057110)
Read-pairs per sample
Read-pairs per Sample, Gene-Level
Exon Bins and Junction Sites
Exons
known transcripts
full length CNTRL (270kDa)
Exons 11 15 16
N
Nud1p / Cdc11p
TACC
Stathmin
TACC
C
127 233 435 623 879 913 1385 1658 2325
Stathmin-domain required for regulation of mitotic spindle assembly
AA1951-2121 required for centrosome localization
CNTRL with Exon11 alternative 3'UTR usage (110kDa)
N
Nud1p / Cdc11p
TACC
C
1 127 233 435 559
D
Clspn
Mean normalized coverage (ENSMUSG00000042489)
Read-pairs per sample
Read-pairs per Sample, Gene-Level
Exon Bins and Junction Sites
Exons
known transcripts
126580000 126570000 126580000 126590000
CLSPN
CHK1-binding domain
N
replication fork interacting domain
CHK1-activating domain
CKB motif1
CKB motif2
CKB motif3
C
1 273 622 773 887 896 905 917 926 954 963 1336
Exon12
E
K14
Hoechst
K1
merge
K14 K1

Figure S3. Confirmatory experiments on functional relevance of RNAseq analysis. Related to Figure 3

(A) Immunofluorescence staining for BrdU (green) 24h after pulsing.

(B) Immunofluorescence stainings for ITGB4 Integrin (green), Ki67 (red), and nuclei (blue) from control and *Egfr*$^{\Delta ep}$ mice at indicated timepoints, showing IFE.

(C) JunctionSeq diagram of exon and junction site usage within the *Cntrl* gene (top). Purple coloured exons and junction sites show significantly differentially used elements. Schematic drawing of protein domains of *Cntrl* (bottom).

(D) JunctionSeq diagram of exon and junction site usage within the *Clspn* gene (top). Purple coloured exons and junction sites show significantly differentially used elements. Schematic drawing of protein domains of *Clspn* (bottom).

(E) Immunofluorescence staining for K14 (green), K1 (red) and nuclei (blue) of primary keratinocytes. Bars 10µm.

Scale bars 20µm unless otherwise stated.

Fig. S4, Amberg et al

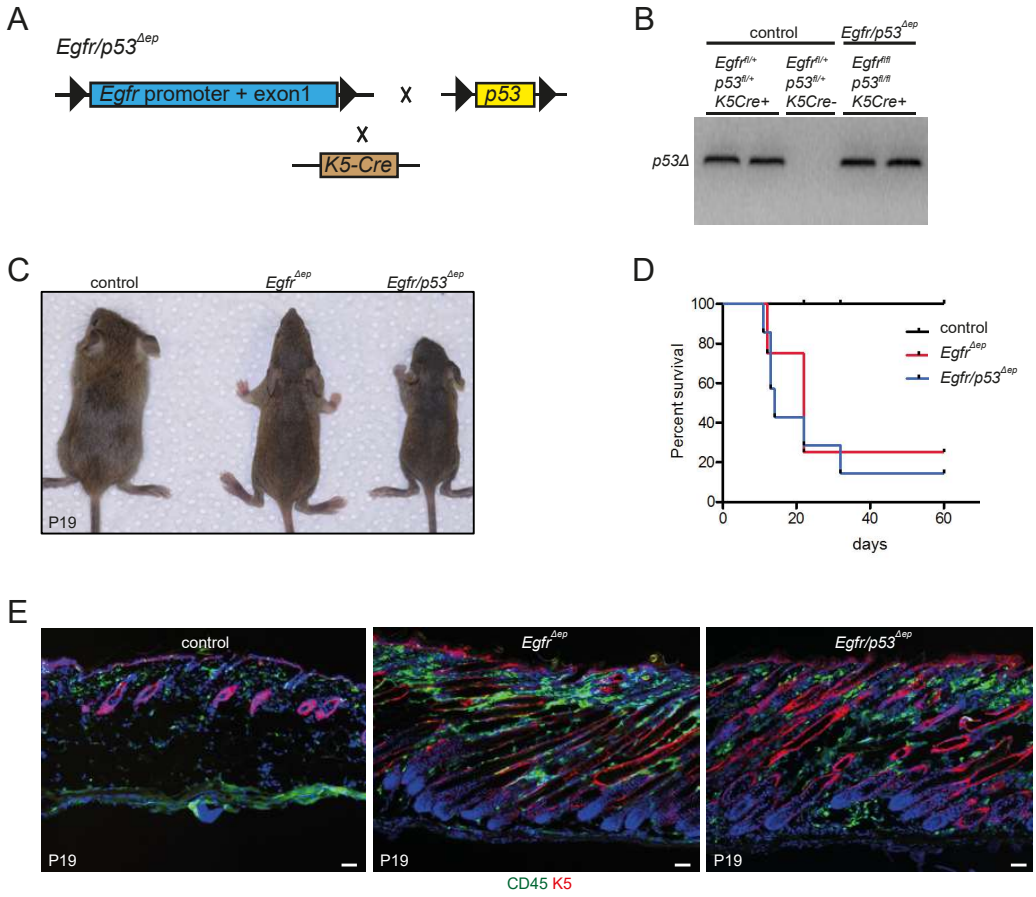

Figure S4. Additional deletion of TP53 does not rescue survival and hair phenotype of mice with EGFR-deficient epidermis. Related to Figure 4

(A) Schematic representation of genetics of *Egfr/p53*$^{\Delta ep}$ mice.
(B) Agarose gel image of *p53* Δallele-specific PCR from control and *Egfr/p53*$^{\Delta ep}$ mice.
(C) Photographs of P19 control, *Egfr*$^{\Delta ep}$ and *Egfr/p53*$^{\Delta ep}$ mice.
(D) Survival curves of control, *Egfr*$^{\Delta ep}$ and *Egfr/p53*$^{\Delta ep}$ mice. Each line shows data from n = 15 mice per genotype.
(E) Immunofluorescence staining of back skin sections for CD45 (green), K5 (red) and nuclei (blue) of P19 control, *Egfr*$^{\Delta ep}$ and *Egfr/p53*$^{\Delta ep}$ mice.

Scale bars 50μm.

Fig. S5, Amberg et al

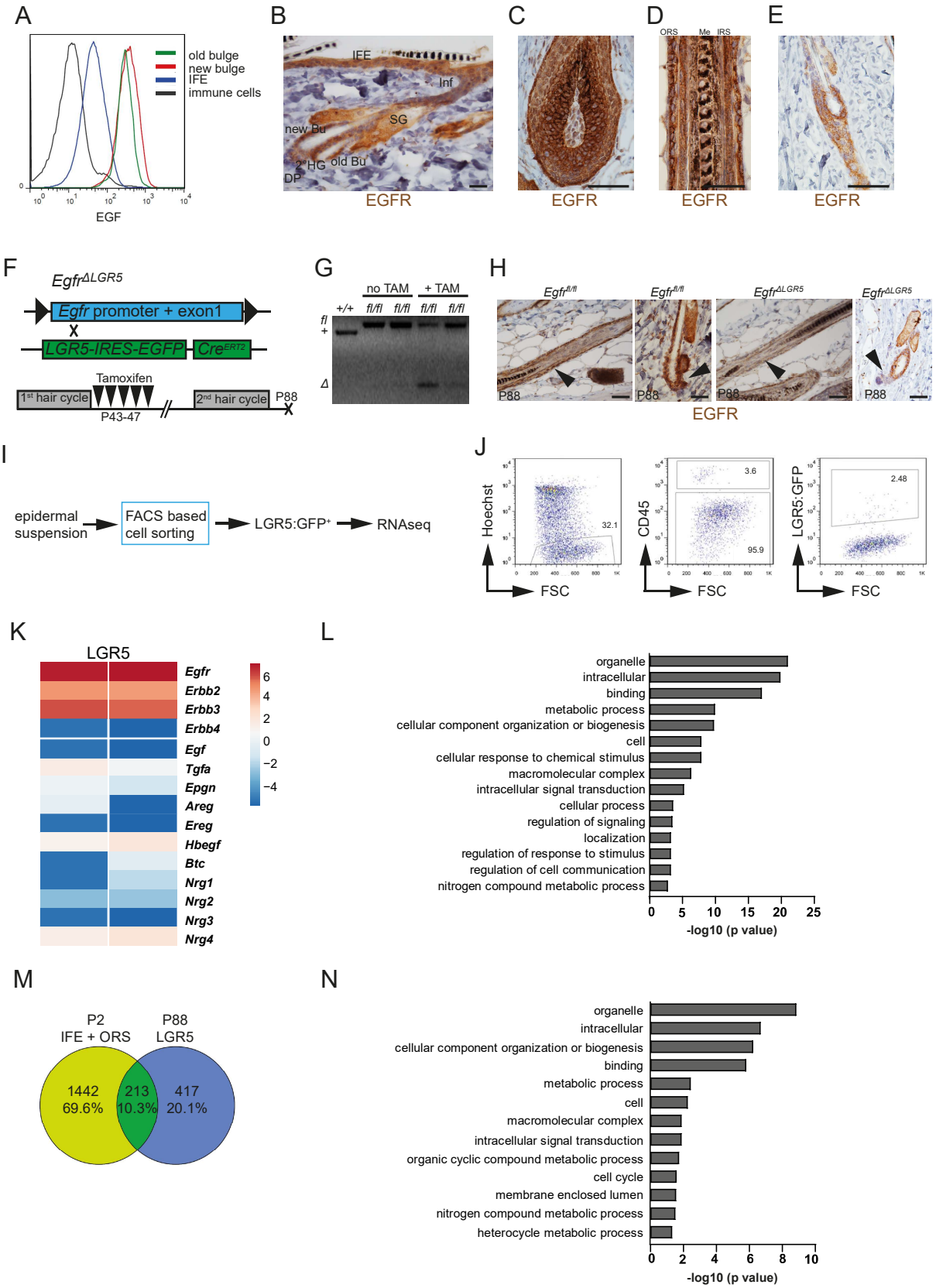

Figure S5. Analysis of localization and function of EGFR in the epidermis of adult mice. Related to Figure 6

(A) Histogram from FACS analysis of P45 mice showing intensity of EGF-A647 for indicated epidermal compartments.

(B) Immunohistochemistry staining of EGFR on a back skin section of an adult control mouse. IFE – interfollicular epidermis; Inf – Infundibulum; SG – sebaceous gland; Bu – bulge; 2°HG – secondary hair germ; DP – dermal papilla.

(C) Immunohistochemistry staining of EGFR on a back skin section of an adult control mouse, showing the matrix of an anagen HF.

(D) Immunohistochemistry staining of EGFR on a back skin section of an adult control mouse, showing the hair shaft of an anagen HF; ORS – outer root sheath; Me – medulla; IRS – inner root sheath.

(E) Immunohistochemistry staining of EGFR on a back skin section of an adult control mouse, showing a catagen HF.

(F) Schematic representation of genetics of *Egfr*$^{\Delta LGR5}$ mice and treatment regimen.

(G) Agarose gel image of *Egfr* Δ-allele specific PCR from back skin of control and *Egfr*$^{\Delta LGR5}$ mice.

(H) Immunohistochemistry staining of back skin sections of P88 control and *Egfr*$^{\Delta LGR5}$ mice, showing anagen and telogen HFs.

(I) Schematic overview of work flow for RNAseq.

(J) FACS gating strategy for cell sorting of LGR5^{+} cells from P88 control and *Egfr*$^{\Delta LGR5}$ mice.

(K) Heat map showing expression of *Erbb* receptors and their ligands from control samples of P88 LGR5^{+} HFSCs. Each column represents one mouse.

(L) Bar diagram of top 15 GO terms of alternatively used exons and junction sites of LGR5^{+} cells from P88 *Egfr*$^{\Delta LGR5}$ mice.

(M) Venn diagram of alternatively spliced genes from P2 IFE + ORS and P88 LGR5^{+} cells.

(N) Bar diagram of GO terms of shared alternatively spliced genes between P2 IFE + ORS and P88 LGR5^{+} cells.

Scale bars 20μm unless otherwise stated.

Transparent Methods

Mice

Mice were kept in the animal facilities of the Medical University of Vienna in accordance with institutional policies and federal guidelines. Animal experiments were approved by the Animal Experimental Ethics Committee of the Medical University of Vienna and the Austrian Federal Ministry of Science and Research (animal license numbers: GZ 66.009/124-BrGT/2003; GZ 66.009/109-BrGT/2003; BMWF-66.009/0073-II/10b/2010; BMWF-66.009/0074-II/10b/2010). $EGFR^{fl/fl}$ mice (Natarajan et al. 2007) were kept in C57BL/6 background for more than 30 generations and were crossed with K5Cre transgenic mice (Tarutani et al. 1997), (LGR5-EGFP-Cre^{ERT2} knock-in mice (Barker et al. 2007) and $p53^{fl/fl}$ mice (Marino et al. 2000). While K5Cre and LGR5-EGFP-Cre^{ERT2} mice were of C57BL/6 background, $p53^{fl/fl}$ mice were of mixed background. Sequences of genotyping primers can be found in Supplemental Table S2.

No phenotypic differences have been identified between male and female mice, thus all experiments were conducted using both genders. Age of analysed mice is indicated in each figure legend.

Embryonic and newborn pups were sacrificed by decapitation. Mice older than P3 were sacrificed by cervical dislocation.

For Tamoxifen-induced deletion of EGFR, 1mg Tamoxifen/mouse (resolved in 10v/v% EtOH (Roth) and 90v/v% sun flower seed oil (Sigma) was injected for 5 consecutive days from P43-47.

Keratinocyte culture

Back skin was surgically removed and subcutaneous adipose tissue was gently removed. Skin was placed dermal-side down on 0.8% Trypsin (diluted in PBS, Sigma) at 37°C for 30min. Epidermis was peeled off under a sterile laminar flow hood, transferred to a 1.5ml Eppendorf tube containing PBS + 2% chelated FCS and chopped into tiny pieces using sterile scissors. This solution was transferred to 15ml Falcon tube and after adding 5ml DNaseI solution (Sigma, #DN25, 250µg/ml in MEM + 8% chelated FCS) incubated on a rotating shaker at 37°C for 45min. 10ml PBS + 2% chelated FCS were added and the solution was pipetted up and down several times and passed over a 70µm cell strainer into a new tube. After centrifugation at 300g for 10min, cells were resuspended in keratinocyte medium (PromoCell, medium constituted according to the manufacturer's instructions), counted and incubated at a concentration of $5x10^4$ cells/well in pre-coated 8-well chamber slides at 32°C (Coating medium: 100ml MEM, 10ml BSA (FractionV 1mg/ml), 1ml 2mM HEPES pH 7.3, 1ml PureCol (Inamed BioMaterials), 1ml 1mg/ml Fibronectin, 1.16ml 100mM $CaCl_2$). 24-36 hours later, medium was changed and cells were allowed to grow for 2-3 more days.

BrdU incorporation assay

For *in vivo* ORS BrdU incorporation assays, newborn mice were injected with 0.625mg BrdU once and sacrificed 24h later. For IFE BrdU incorporation assays, mice of 5, 8, or 10 days of age were injected with BrdU and sacrificed 4h later.

Histology (Sections)

For histological analysis, skin was processed as described previously (Amberg et al. 2015). Briefly, paraffin-embedded skin biopsies were cut into 4µm thin sections and stained with Hematoxylin & Eosin or Fontana Masson according to standard protocols or subjected to immunohistochemistry (IHC) stainings. For IHC, samples were deparaffinized and rehydrated, antigen retrieval was performed using the respective antigen retrieval buffer and an aptum Retriever 2100 antigen retrieval machine. Endogenous peroxidase was blocked by incubation in 3% H_2O_2 in Methanol for 10min, followed by biotin blocking using Endogenous Biotin Blocking Kit (LifeTech) for 20min each and blocking of unspecific antibody binding using PBS supplemented with 1% BSA, 5% Horse Serum and 0.1% Triton X-100 for 1h at room temperature before adding primary antibodies. In case primary antibodies were raised in mouse, blocking was performed using M.O.M. kit (mouse on mouse, Vector Laboratories, FKM-2201). Primary antibodies were incubated in antibody blocking buffer (1% BSA, 5% Horse Serum, 0.1% TritonX-100 in PBS) over night at 4°C. Biotinylated secondary antibodies were diluted 1:500 in antibody blocking buffer and incubated at room temperature for 1h, followed by Streptavidin incubation for 30min. After DAB reaction was performed, sections were counterstained with Gill's Hematoxylin, dehydrated and embedded using Entellan.

For BrdU stainings, 4µm paraffin sections were incubated with 1N HCl at 37°C for 1h, blocked with antibody blocking buffer and stained with anti-BrdU antibody (BD, 1:50) at 4°C over night. Secondary antibody was diluted 1:500 in blocking buffer, and together with Hoechst (1µg/ml) incubated for 1h at room temperature, before mounting with DAKO mounting medium.

In order to obtain frozen samples, skin biopsies were embedded in Sakura O.C.T., frozen on dry ice and stored at -80°C until sectioning in a Histocom cryomicrotome. 6µm sections were stored at -80°C until further use. For GFP staining, fresh skin biopsies were fixed in 4% PFA for 2h and incubated in 30% sucrose in PBS at 4°C over night prior to embedding and freezing in Sakura O.C.T. Frozen sections were thawed, blocked with 4% PFA for 10min at room temperature, incubated with antibody blocking buffer for 1h at room temperature and stained with primary antibody diluted in antibody blocking buffer at 4°C over night. Secondary antibodies were diluted 1:500 in blocking buffer, and together with Hoechst (1µg/ml) incubated for 1h at room temperature, before mounting with DAKO mounting medium.

Sections were all imaged at a Nikon Eclipse i80 microscope using NIS Elements software (equipped with a Nikon DS-U2 camera for brightfield microscopy and a Nikon DS-Qi2 camera for epifluorescence microscopy), a Zeiss Axio Imager using Axio Vision software or a Zeiss LSM700 confocal microscope using ZEN2010. Images were further processed using Photoshop5.

Histology (Transmission electron microscopy)
Back skin biopsies were cut into pieces of 1x1 mm, fixed in 3% glutaraldehyde (AGAR Scientific) in 0.1M caco buffer (AGAR Scientific), post-fixed in 1 % osmium tetroxide (EMS), dehydrated and embedded in Agar Low Viscosity resin (AGAR Scientific). 80nm ultrathin sections were performed at a Reichert-Jung Ultracut E microtome and stored on copper grids (AGAR Scientific).Sections were further stained in 0.5% uranyl acetate (Laurylab) and 3% lead citrate (Laurylab) before imaging at a TEM Philips *I* FEI EM 208 or a TEM ZEISS EM 902.
Histology (primary keratinocytes)
Medium was removed and cells were washed with PBS 3 times. Cells were incubated with 4% PFA for 30min at RT, washed with PBS 3 times and staining procedure was identical to histological sections. Phalloidin-A488 was diluted 1:1000. Images were acquired at a Zeiss LSM700 confocal microscope, using ZEN2010 software.

Flow cytometry
Epidermal cell suspensions were generated by surgically removing the trunk skin and gently scraping off subcutaneous adipose tissue. Skin was then placed on DMEM (Gibco) containing 2mM EDTA and 0.25% Trypsin (Gibco) at 4°C over night. Next day, epidermis was softly scraped off and further dissociated into single cells by pipetting up and down after adding DMEM containing 2% chelexed FCS (Sigma). Cells were filtered using 70µm and 40µm cell strainers (BD), centrifuged at 300g for 10min, and washed with PBS (Sigma) containing 2% chelexed FCS twice before staining. Epidermal single cell suspensions were incubated with the following antibodies: a6-PE (BD, 1:50), Scal-PECy7 (Biolegend, 1:100), CD45-APCCy7 (BD, 1:200), CD34-biotinylated (eBioscience, 1:50), Streptavidin-APC or Streptavidin-A700 (BD or LifeTech, 1:400). A647-labelled EGF was purchased from LifeTechnologies and incubated in a dilution of 1:20 for 30min on ice in an additional step after antibody staining. Dead cell exclusion was performed using Hoechst (1µg/ml). BrdU analysis was performed according to the manufacturer's instructions (BD APC BrdU Flow Kit, Cat# 552598). For evaluation of $BrdU^+$ cell numbers and intensity measurement of EGF-A647, a BD Fortessa cytometer with BD FACSDiva software was used. Further analysis was conducted using FlowJo (Trestar) software. Cell sorting of IFE and ORS cell populations from P2 skin, as well as of P88 $LGR5^+$ HFSCs was performed using a BD AriaI and BD FACSDiva software.

RNA isolation
Approx. 8,000 IFE and 1,000 $LGR5^+$ keratinocytes were sorted into RNA Extraction Buffer of the PicoPure RNA Isolation Kit (Arcturus), incubated at 42°C for 30min and centrifuged at 800g for 2 min. Supernatants were transferred into new tubes and stored at -80°C until further RNA purification according to the manufacturer's instructions, despite the last step. For RNA elution, we did not use the provided Elution Buffer, but RNase-free water in order to be able to measure RNA quality with the BioAnalyzer (Total Eukaryote RNA Pico Kit, Agilent, according to the manufacturer's instructions).

Library Preparation
RNA samples with RIN > 8.0 were used for RNAsequencing. Libraries were prepared using SMARTer Ultra Kit (Clontech, #63482) and Low Input Library Prep Kit (Clontech, #634947) according to the manufacturer's instructions.

Libraries were subjected to paired-end 150bp read RNAseq at the Biomedical Sequencing facility of the CEMM (Vienna, Austria) using the HiSeq2500 (Illumina Inc.).

RNAseq analysis
TopHat2 algorithm was used to align raw RNA-seq data to mm10 (Kim et al. 2013). Differentially expressed genes were identified using DeSeq2 algorithm (Love et al. 2014). An adjusted P<0.1 was defined as cutoff for differentially expressed genes. Gene Ontology analyses were performed using Ontologizer software (Bauer et al. 2008). Differential splicing was analyzed using the R package JunctionSeq (Hartley and Mullikin 2016).

Data availability
Raw data from RNAseq experiments are available at the NCBI Gene Expression Omnibus (GEO) with the GEO accession number GSE128436.

qRT-PCR
cDNA was generated using VILO cDNA synthesis kit (Life Technologies) according to the manufacturer's protocol. cDNA was stored at -20°C until further use. qRT-PCR was run with SYBR green (Peqlab) on an ABI7500 qRT-PCR machine under the following conditions: an initial incubation at 50°C for 20sec and 95°C for 10 min followed by 40 cycles of 95°C for 15sec, 54°C for 1 min. Relative quantification of RNA was calculated by the $\Delta\Delta C_t$ method using *Gapdh* as reference gene. Primer sequences were purchased from MWG Eurofins.

Statistics
Data were analysed by two-tailed Student's t test, Kruskal-Wallis test or multiple t-tests according to Two-stage linear step-up procedure of Benjamini, Krieger and Yekutieli with Q = 1%. Error bars represent ±SD. Exact number of animals and samples are stated in the figure legends. P values less than 0.05 were considered significant, with $p< 0.05$ *, $p < 0.01$ **, $p < 0.001$ ***.

Polar Plots
Polar plots were generated using R software.

Supplemental References

Amberg N, Holcmann M, Glitzner E, Novoszel P, Stulnig G, Sibilia M. 2015. Mouse Models of Nonmelanoma Skin Cancer. in *Methods in Molecular Biology*, pp. 217-250. Springer Science + Business Media.

Barker N, van Es JH, Kuipers J, Kujala P, van den Born M, Cozijnsen M, Haegebarth A, Korving J, Begthel H, Peters PJ et al. 2007. Identification of stem cells in small intestine and colon by marker gene Lgr5. *Nature* **449**: 1003-1007.

Bauer S, Grossmann S, Vingron M, Robinson PN. 2008. Ontologizer 2.0--a multifunctional tool for GO term enrichment analysis and data exploration. *Bioinformatics* **24**: 1650-1651.

Hartley SW, Mullikin JC. 2016. Detection and visualization of differential splicing in RNA-Seq data with JunctionSeq. *Nucleic Acids Res* **44**: e127.

Kim D, Pertea G, Trapnell C, Pimentel H, Kelley R, Salzberg SL. 2013. TopHat2: accurate alignment of transcriptomes in the presence of insertions, deletions and gene fusions. *Genome Biol* **14**: R36.

Love MI, Huber W, Anders S. 2014. Moderated estimation of fold change and dispersion for RNA-seq data with DESeq2. *Genome Biol* **15**: 550.

Marino S, Vooijs M, van Der Gulden H, Jonkers J, Berns A. 2000. Induction of medulloblastomas in p53-null mutant mice by somatic inactivation of Rb in the external granular layer cells of the cerebellum. *Genes Dev* **14**: 994-1004.

Natarajan A, Wagner B, Sibilia M. 2007. The EGF receptor is required for efficient liver regeneration. *Proceedings of the National Academy of Sciences* **104**: 17081-17086.

Tarutani M, Itami S, Okabe M, Ikawa M, Tezuka T, Yoshikawa K, Kinoshita T, Takeda J. 1997. Tissue-specific knockout of the mouse Pig-a gene reveals important roles for GPI-anchored proteins in skin development. *Proceedings of the National Academy of Sciences* **94**: 7400-7405.